Partitioning And Transmuter Research Initiative in a Collaborative Innovation Action

PATRICIA

Grant Agreement Number 945077

Research and Innovation Action

Activity: NFRP-2019-2020

Topic: NFRP-2019-2020-07 Safety Research and Innovation for Partitioning and/or Transmutation

Start date: 01/09/2020 – Duration: 48 months

DELIVERABLE

D5.1 Description of new correlations and databases for fuel performance codes to be applied to Am bearing fuels

Authors: P. Van Uffelen, A. Schubert (JRC), M. Lainet (CEA), A. Magni, M. Di Gennaro, M. Guarnieri, D. Pizzocri, L. Luzzi (POLIMI)

This project has received funding from the European Union's Horizon 2020 research and innovation programme under grant agreement No 945077.

DOCUMENT CONTROL SHEET

DOCUMENT INFORMATION	
Document title	Description of new correlations and databases for fuel performance codes to be applied to Am bearing fuels
Author(s), (organization)	P. Van Uffelen, A. Schubert (JRC), M. Lainet, (CEA), A. Magni, M. Di Gennaro, M. Guarnieri, D. Pizzocri, L. Luzzi (POLIMI)
Document type	Deliverable
Document ID	D5.1
Work package n°	WP5 (Domain: Transmutation)
Work package title	WP5 (WP22) Improvement of modelling and fuel performance codes
Lead beneficiary	JRC
Dissemination level	Public
Date of issue	09/02/2024
Archive ID reference COO	

DOCUMENT SUMMARY

In this deliverable, we outline the correlations and data that have been transferred to models suitable for fuel performance codes (TRANSURANUS, GERMINAL) for the simulation of Am-bearing oxide fuels. This is based on the information provided in the open literature in addition to the results obtained in Work Package 4 of the PATRICIA project. The objective was to derive advanced laws for thermal-mechanical properties, based on both experimental and lower-length data in order to improve the accuracy and physical basis of the fuel performance codes (FPCs) for safety analyses.
The safety-relevant oxide fuel properties implemented include: (i) advanced models for the melting (solidus) temperature of Am-bearing fuels implemented in TRANSURANUS; (ii) state-of-the-art and advanced models for the thermal conductivity of Am-bearing fuels implemented in both the FPCs; (iii) heat capacity models for MOX fuels extended to account for the fuel Am content; and (iv) a more mechanistic model for oxide fuel creep in TRANSURANUS. The first two properties benefited from the developments in WP4 based on atomic-scale and CALPHAD simulations.

For what concerns the cladding properties, dedicated correlations for the MYRRHA cladding steel (DIN 1.4970, of the 15-15Ti steels family) were implemented in TRANSURANUS and used for MYRRHA simulations. More precisely, the models considered target the thermal and irradiation-induced creep, void swelling and time-to-rupture, applicable to ranges relevant for the current MYRRHA core design.

For what concerns thermo-physical properties of the LBE coolant, advanced correlations are also implemented in TRANSURANUS. On the one hand, the thermal conductivity, specific heat, density and viscosity correspond to the recommendations provided by the latest NEA Handbook. On the other hand, the heat transfer coefficient between cladding and coolant is modelled in TRANSURANUS via the Ushakov correlation as a standard. Other correlations suitable for LBE, from Subbotin and Kazimi-Carelli, have also been implemented in the TRANSURANUS code for a sensitivity analysis.

Finally, it should be mentioned that the modelling improvements of the SCIANTIX module, coupled with the TRANSURANUS and GERMINAL codes for a more mechanistic description of inert gas behaviour and fuel microstructure evolution, are outlined separately in the Deliverable 5.2.

DOCUMENT HISTORY		
Version	**Status**	**Date**
V1	Final	09/02/2024

DOCUMENT APPROVAL The author, WP Leader and Coordinator acknowledge and accept delivery of the work completed for this deliverable.		
Date	**Author(s)**	**Organisation**
09/02/2024	Paul Van Uffelen, Arndt Schubert Marc Lainet Alessio Magni, Martina Di Gennaro, Mattia Guarnieri, Davide Pizzocri, Lelio Luzzi	JRC CEA POLIMI
Date	**WP Leader**	**Organisation**
16/02/2024	Lelio Luzzi	POLIMI
Date	**Coordinator**	**Organisation**
	Paul Schuurmans	SCK CEN

DISTRIBUTION LIST		
Project Officer Renata Bachorczyk-Nagy	EC	Copy on PATRICIA SharePoint
PATRICIA Beneficiaries	PATRICIA Consortium	

Table of contents

1 Introduction

Fuel performance codes (e.g., TRANSURANUS [1, 2], GERMINAL [3, 4]) are essential computational tools for the design optimization, assessment and safety analyses of fuel pins for reactor core concepts. They are applied within the European Project PATRICIA [5] to advanced, mixed-oxide (MOX) fuelled pins for fast reactor irradiation. In particular, the PATRICIA target is the behaviour of pins loaded with Am-bearing oxide fuels for irradiation in the MYRRHA reactor ("Revision 1.8"), with transmutation purposes. The current option for MYRRHA driver fuel irradiation consists of U-Pu-Am-O fuel with Am content in the range [0 – 5] at.% [6] and a total content of Pu and Am of 30 at.%. Additionally, blanket fuel concepts are of interest for advanced reactor designs, targeting the periphery of fast reactor cores. This fuel option currently corresponds to U-Am-O with higher Am contents > 10 at.% [7].

The reliable application of fuel performance codes to these advanced fuel concepts for fast reactor application requires the development of extended and dedicated models for fuel properties, which need to be engineering-level and suitable for code implementation and use. Moreover, the properties and behaviour under irradiation of fast reactor-type cladding materials (stainless steels) and coolants (liquid metals) must be properly modelled, since contributing to the overall pin performance both during normal operation and transient / accidental conditions.

For these reasons, modelling advancements were carried out in the frame of PATRICIA, which are implemented in the fuel performance codes to extend their applicability and assessment to a broader set of fuel materials and fast reactor irradiation conditions. The next section of this deliverable focuses on novel models for thermal properties of fast reactor-type, mixed-oxide fuels: melting (solidus) temperature, specific heat capacity, thermal conductivity, and fuel creep. Section 3 is dedicated to the models for the behaviour under irradiation of the cladding selected for the MYRRHA reactor design (DIN 1.4970), while Section 4 reports the models newly implemented in TRANSURANUS for the properties and heat transfer capability of lead-bismuth eutectic (LBE), chosen as a coolant for MYRRHA. The correlation for thermal conductivity of minor actinide-bearing oxide fuels has also been incorporated in the GERMINAL code in the frame of the PATRICIA project.

In section 5, we summarise some discussions held between partners from POLIMI, CEA, TUDelft and JRC involved in transferring results from Work Package (WP) 4 (devoted to deriving data on the thermo-chemical properties of minor actinide-bearing fuels) to WP5, and in the final section we summarise the outcome of model recommendations for the considered properties towards the use in fuel performance codes applied to pin performance simulations.

2 Models for fuel properties

Thermal properties of fast reactor-type mixed-oxide fuels were targeted by modelling advancements on the basis of data and information available in literature and via the PATRICIA Project. The focus was on melting temperature, specific heat and thermal conductivity, since fundamental properties determining the margin to fuel melting (safety limit to which any design must comply with) and more generally the fuel thermal performance both during reactor normal operation conditions and under power / temperature transients. The fuel materials targeted in the framework of PATRICIA are Am-bearing oxides for transmutation purposes, as already mentioned in the Introduction.

While a low Am concentration in the fuel ("homogeneous", within [0, 5] wt.%) would allow the use of models for U-Pu-O fuels (already available / previously implemented in TRANSURANUS, e.g., [1, 8-10]) also for U-Pu-Am-O fuels, given the limited impact on the fuel properties compared to U-Pu-O [11-13], a dedicated modelling proves necessary to target oxide fuels bearing higher amounts of minor actinides (within [10 – 20] wt.%), for e.g., blanket fuel and transmutation purposes [7].

2.1 Melting (solidus) temperature modelling

The model already available in TRANSURANUS v1m4j22 [14] and used for pin performance simulations in the PATRICIA Project corresponds to the one developed, assessed and published in [15], reading:

$$\mathrm{T_{m,0}(x, [Pu], [Am]) = T_{m,UO_2} - \gamma_x\, x - \gamma_{Pu}\, [Pu] - \gamma_{Am}\, [Am]} \qquad (1)$$

$$\mathrm{T_m(x, [Pu], [Am], bu) = T_{m,inf} + (T_{m,0} - T_{m,inf}) \cdot e^{-\frac{bu}{\delta}}} \qquad (2)$$

where $\mathrm{T_{m,UO_2}}$ is the melting temperature of fresh stoichiometric UO_2, i.e., 3147 K according to the experimental measurements by Manara et al. [16], recommended by the ESNII+ Catalogue on MOX properties [17]; x is the deviation from fuel stoichiometry, while $\mathrm{[Pu]}$, $\mathrm{[Am]}$ are the plutonium and americium contents, respectively. bu is the fuel burnup in GWd/t_{HM}, $\mathrm{T_{m,0} = T_{m,0}(x, [Pu], [Am])}$ is the melting temperature of fresh minor actinide-MOX according to Eq. 1, while $\mathrm{T_{m,inf}}$ and δ are the correlation parameters representing the burnup degradation effect. The model regressors are specified in [15].

Recent data obtained from a CALPHAD modelling of the U-Pu-Am-O fuel system, including [18] and new computational data provided by Work Package 4 of the PATRICIA Project, currently indicate that:

- The behaviour of the melting temperature of mixed-oxide fuels seems to exhibit a minimum value in the range [60 – 80]% of Pu content, where data are currently missing but an increasing trend is observed for Pu > 80%.
- For a given U-Pu-Am composition, the maximum melting temperature is not at fuel stoichiometry (oxygen-to-metal ratio O/M = 2.00) but at fuel hypo-stoichiometry, and the O/M corresponding to the maximum melting temperature shifts to lower values (stronger hypo-stoichiometry) if the fuel Pu content increases.

Additionally, the melting temperature of U-Am-O fuels has been investigated along the full range of Am contents [19] and on this basis, the effect of the fuel O/M is under investigation within PATRICIA WP4. These results show that the melting temperature decreases when the O/M decreases as well at a fixed americium content.

Due to the different melting behaviour of $(U,Pu,Am)O_{2-x}$ and $(U,Am)O_{2-x}$ according to the novel data mentioned (explicitly recalled in Table 1), two different and dedicated models have been developed for the two different types of Am-bearing fuels. One model describes the solidus temperature of $(U,Pu,Am)O_{2-x}$ homogeneous fuel with Am contents up to 5 at.%, while a second model describes $(U,Am)O_{2-x}$ heterogeneous fuel with Am content of americium up to 20 at.%.

Table 1: Additional datasets considered for the modelling of melting (solidus) temperature of Am-bearing oxide fuels, together with the data already considered in [15].

$(U,Pu,Am)O_{2-x}$		
Reference	**Details**	**Ranges covered**
Kato et al. 2009 [20]	Experimental data on $(U,Pu,Am)O_{2-x}$: database of solidus-liquidus temperatures from literature review	[Pu] = [0, 60] at.% [Am] = [0, 3.5] at.% O/M = [1.93, 2.00]
De Bruycker et al. 2011 [21]	Experimental data on high-Pu $(U,Pu)O_2$	[Pu] = [75, 100] at.% O/M = 2.00
Gueneau et al. 2023 [22]	Experimental data on $(U,Pu,Am)O_{2-x}$: samples PHENIX29-OM + 29-brut, TRABANT40-OM + 40-brut, CAPRA4, TRABANT45	[Pu] = [23.5, 50] at.% [Am] = [0.5, 2] at.% O/M = [1.98, 2.00]
Fouquet-Metivier et al. 2023 [18]	CALPHAD results on $(U,Pu)O_2$ and critical review of experimental data on high-Pu content fuels	[Pu] = [0, 100] at.% O/M = 2.00
PATRICIA WP4	CALPHAD results on $(U,Pu,Am)O_{2-x}$	[Pu] = 30 at.% [Am] = [0, 5] at.% O/M = [1.97, 2.00]
$(U,Am)O_{2-x}$		
Reference	**Details**	**Ranges covered**
Prieur et al. 2016 [23]	Experimental data: laser heating under inert Ar	[Am] = 10, 15 at.% O/M ~ 2.00
Epifano et al. 2020 [24]	Experimental data: laser heating under Ar and air atmospheres	[Am] = [0, 70] at.% O/M ~ 2.00
Labonne et al. 2023 [19]	Atomic-scale data	[Am] = [0, 50] at.% O/M = 2.00
PATRICIA WP4	CALPHAD results	[Am] = 10, 15, 20 at.% O/M = 1.93, 1.94, 1.95

* Analysed but not used for the property modelling, due to relevant uncertainties related to the interpretation of these measurements as solidus or liquidus points (see Section 5.1).

Model for $(U,Pu,Am)O_{2-x}$

The model developed for the solidus temperature of $(U,Pu,Am)O_{2-x}$ describes:

- the behaviour of the U-Pu-O system in a parabolic way, coherently with state-of-the-art literature data covering the entire Pu composition range
- the hypo-stoichiometric O/M corresponding to the maximum solidus temperature as a function of the Pu content, following the indications from atomic-scale and CALPHAD calculations (PATRICIA WP4)
- the degradation of the mixed-oxide solidus temperature as a linear function of the fuel Am content, again based on the recent data provided by PATRICIA WP4.

The resulting model formulation is expressed by Eq. 3, which holds for fresh fuels. The burnup degradation (extending the model to irradiated fuels, Eq. 4) is assumed to be in line with the model already assessed in [15], with model parameters re-fitted on the extended and updated dataset considered in this work (Table 1).

$$\begin{aligned} T_{m,0}([Pu],[Am],O/M) & \\ &= T_{m,UO_2} + C_1[Pu] + C_2[Pu]^2 - (C_1[Pu] + C_2[Pu]^2)\frac{|O/M - O/M_{max}|}{2 - O/M_{max}} \\ &+ (B_1[Pu] + B_2[Pu]^2)\frac{|O/M - O/M_{max}|}{2 - O/M_{max}} - 187.5\,[Am] \end{aligned} \tag{3}$$

$$T_m([Pu],[Am],O/M,bu) = T_{m,inf} + (T_{m,0} - T_{m,inf}) \cdot e^{-\frac{bu}{\delta}} \tag{4}$$

where $T_{m,UO2}$ = 3132 K, updated based on the more recent and widely recommended data from Kato et al. [20]. The Am content effect is calibrated based on the data analysis, resulting in an associated coefficient consistent with existing literature indications [12, 13, 25-27]. The results of the data fitting procedure in terms of regressor values and associated standard errors are collected in Table 2. The proposed formulation of the model is confirmed by a statistical analysis based on the p-values associated to the model regressors, according to the same approach adopted in [15] (i.e., p-value < 5% threshold for the exclusion of a certain effect from the model).

Table 2: Results of the best fit of the statistically-assessed correlation for the melting (solidus) temperature of $(U,Pu,Am)O_{2-x}$ (Eqs. 3 and 4).

Regressor	Units	Estimate	Std. Error
B_1	K at./$^{-1}$	−506.56	17.53
B_2	K at./$^{-2}$	414.91	21.75
C_1	K at./$^{-1}$	−222.84	42.29
C_2	K at./$^{-2}$	132.12	56.14
$T_{m,inf}$	K	2924.53	17.38
δ	GWd/t	65.52	16.79

The model is applicable in the following ranges: [Pu] = [0, 100] at.% (extended to the entire Pu composition range), [Am] = [0, 5] at.%, O/M = [O/M_{max}, 2.00] in the hypo-stoichiometric range (O/M_{max} is modelled as a decreasing function of the fuel Pu content, i.e., $O/M_{max} = 2.00 - 0.235 \cdot [Pu]$), bu = [0, 150] GWd/t.

Some graphical representations of the model behaviour and its verification against the fitted data are provided in Figure 1.

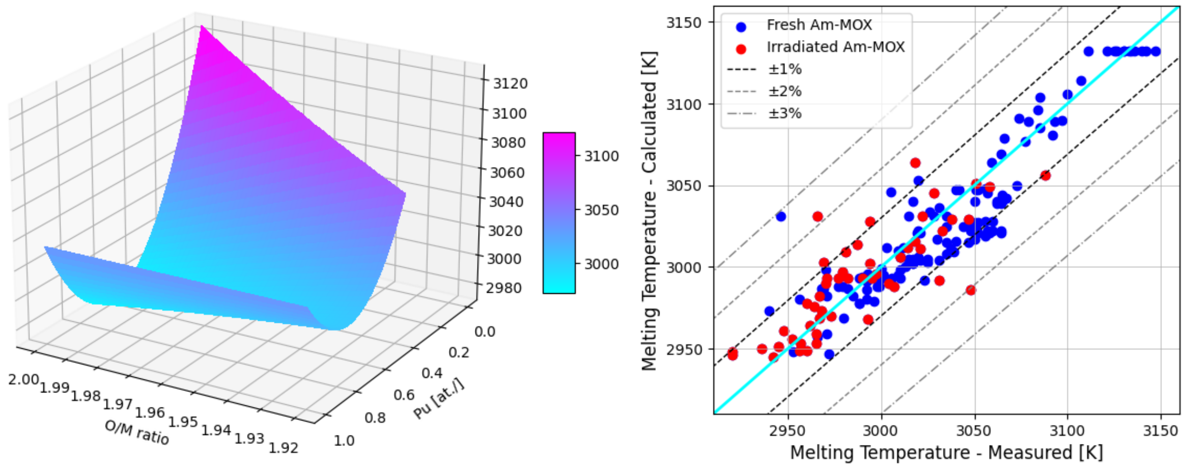

Figure 1: Left: 3D plot of the melting temperature [K] of $(U,Pu,Am)O_{2-x}$ according to the novel model proposed, as a function of O/M ratio and Pu content, for 3% Am content. Right: Comparison of the model predictions with the data considered.

Model for $(U,Am)O_{2-x}$

The data on solidus temperature of $(U,Am)O_{2-x}$ provided by WP4, together with literature data on UO_2 (here considered as a limit fuel system to be coherently reproduced), support the modelling of the property as linearly decreasing with both increasing Am content and deviation from perfect stoichiometry. Hence, the model is formulated as:

$$\mathrm{T}_{\mathrm{m},0}([\mathrm{Am}], \mathrm{O/M}) = \mathrm{T}_{\mathrm{m,UO_2}} + \mathrm{A}_1[\mathrm{Am}] + \mathrm{A}_2|2 - \mathrm{O/M}| \tag{5}$$

where $T_{m,UO2}$ = 3132 K, again from Kato et al. [20] as for the $(U,Pu,Am)O_{2-x}$ system. The results of the data fitting procedure in terms of regressor values and associated standard errors are collected in Table 3. Again, the proposed formulation of the model is confirmed by a statistical analysis based on the p-values associated to the model regressors [15].

Table 3: Results of the best fit of the statistically-assessed correlation for the melting (solidus) temperature of $(U,Am)O_{2-x}$ (Eq. 5).

Regressor	Units	Estimate	Std. Error
A_1	K at./$^{-1}$	−540.8	23.3
A_2	K	−1858.9	83.9

The model applicability is recommended in the following ranges: [Am] = [0, 21] at.% and O/M = [1.93, 2.00]. No specific data are currently available to model the degradation of the melting temperature of $(U,Am)O_{2-x}$ with increasing burnup. As a preliminary choice to be assessed against dedicated data, the same burnup degradation effect modelled for $(U,Pu,Am)O_{2-x}$ (Eq. 4) can be supposed for the moment.

A showcase of the model behaviour, including the comparison with the reference (available) data, is provided in Figure 2.

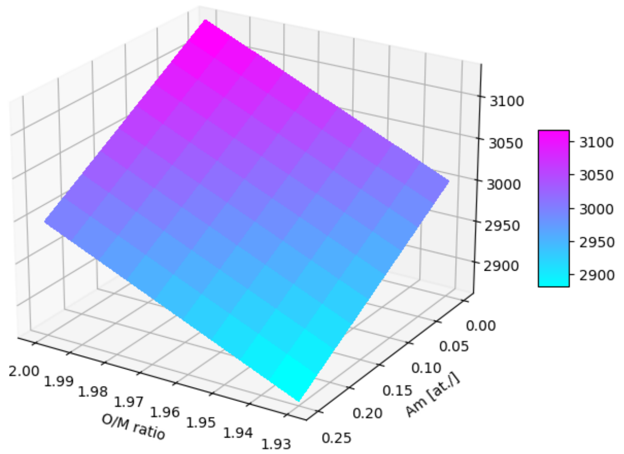

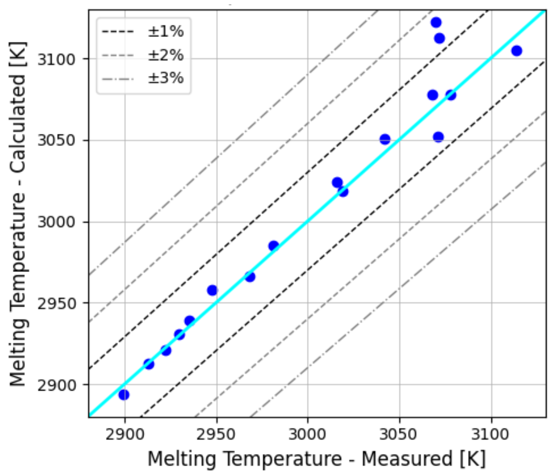

Figure 2: Left: 3D plot of the melting temperature [K] of $(U,Am)O_{2-x}$ according to the novel model proposed, as a function of O/M ratio and Am content. Right: Comparison of the model predictions with the data considered.

2.2 Thermal conductivity modelling

The model already available in TRANSURANUS v1m4j22 [14] as a reference for minor actinide-bearing oxide fuels, used for pin performance simulations in Task 5.3 (fuel performance code benchmark) of the PATRICIA Project, and implemented also in GERMINAL, corresponds to the one developed, assessed and published in [15], reading:

$$k_0(T, x, [Pu], [Am], [Np], p) = \left(\frac{1}{A + BT} + \frac{D}{T^2} e^{-\frac{E}{T}}\right) (1 - p)^{2.5} \tag{6}$$

$$k(T, x, [Pu], [Am], [Np], p, bu) = k_{inf} + (k_0 - k_{inf}) \cdot e^{-\frac{bu}{\varphi}} \tag{7}$$

with $A = A_0 + A_x \cdot x + A_{Pu}[Pu] + A_{Am}[Am] + A_{Np}[Np]$ and $B = B_0 + B_{Pu}[Pu] + B_{Am}[Am] + B_{Np}[Np]$, i.e., with the Am and Np content effects introduced both in the A and B parameters of the lattice vibration contribution to thermal conductivity, in line with preliminary indications provided in [12, 13, 25-27]. The introduction of the minor actinide effects in the lattice vibration contribution to thermal conductivity is confirmed by statistical analyses based on the p-values of the associated regressors [15].

The variable T is for the temperature (K), x is the deviation from fuel stoichiometry, p is the porosity (/), while [Pu], [Am], [Np] are the plutonium, americium and neptunium (local) concentrations, respectively. Then, in Eq. 7 expressing the thermal conductivity of irradiated mixed-oxides (k, coherent with k_0 if the burnup is null): $k_0 = k_0(T, x, [Pu], [Am], [Np], p)$ is the thermal conductivity of fresh fuel calculated using Eq. 6, bu is the fuel burnup in GWd/t_{HM}, k_{inf} is the asymptotic thermal conductivity at high fuel burnup and φ is a model coefficient fitted on irradiated fuel data. The model regressors are specified in [15].

Modelling advancements on the Am-bearing oxide fuel thermal conductivity within PATRICIA rely on the same physically-grounded models as a basis, but accounting for new recent literature data and approaches (e.g., [28-33]) and on in-house data on the $(U,Am)O_2$ thermal diffusivity shared by JRC-Karlsruhe [34]. These data support an advanced theoretical analysis of the thermal diffusivity (and hence, conductivity) of $(U,Am)O_{2-x}$, by comparing the effect of Am impurities to that of (trivalent) lanthanides in solid solutions in UO_2, as investigated in [35]. The effect of variation of the atomic mass and lattice strain due the lanthanides / americium inserted in the fuel matrix proves relevant on the material thermal diffusivity, with trivalent Am(III) significantly changing the conductivity of the oxide matrix. In particular, a homogeneous inclusion of Am in the lattice induces a stronger interaction with the phonons compared to a heterogeneous inclusion of "impurities" (which also underlines the importance of the fabrication method of the samples for experimental investigations [33]). The novel thermal diffusivity / conductivity data considered in this work are recalled in the following Table 4.

Table 4: Additional datasets considered for the modelling of thermal conductivity of Am-bearing oxide fuels, together with the data already considered in [15].

$(U,Pu,Am)O_{2-x}$		
Reference	**Details**	**Ranges covered**
Yokoyama et al. 2022 [28-33]	Experimental data: laser-flash device for thermal diffusivity of $(U,Pu,Am)O_2$. Converted to thermal conductivity via specific heat from Kopp's law and density from recommendations	T = [25, 1230]°C [Pu] = [29, 30] at.% [Am] = 5.3, 10.2, 15 at.% O/M = 2.00 p = 10%, 12%, 19%
Gueneau et al. 2023 [22]	Experimental data: shielded laser-flash device for measurements of thermal diffusivity of $(U,Pu)O_2$	T = [270, 1180]°C [Pu] = 32 at.% O/M ~ 2.00 p = 7%
Bonev et al. 2023 [30]	Reports experimental data on irradiated $(U,Pu)O_{2-x}$ NESTOR-3 fuels: laser-flash method for simultaneous thermal diffusivity and specific heat capacity measurements	T = [280, 1230]°C [Pu] = 22 at.% O/M = 1.975 p = [4, 6]% bu = 77 GWd/t
Horii et al. 2024 [33]	Experimental data: laser-flash device for thermal diffusivity measurements on $(U,Pu,Am)O_2$	T = [800, 1400]°C [Pu] = 18 at.% [Am] = 0.5 at.% O/M = 2.00 p = 5.7%
$(U,Am)O_{2-x}$		
Reference	**Details**	**Ranges covered**
Ronchi et al. 1999 [36]	Experimental data: laser-flash method to measure thermal diffusivity of UO_2	T = [300, 2600]°C O/M ~ 2.00 p = 5%
Ronchi et al. 2004 [37]	Experimental data: laser-flash device for simultaneous measurements of thermal diffusivity and specific heat capacity of irradiated UO_2	T = [400, 1020]°C O/M ~ 2.00 p = 5% bu = 34, 51 GWd/t
Valu et al. 2014 [38]	Experimental data: laser-flash method to measure thermal diffusivity of $(U,Am)O_{2-x}$ (after annealing to remove alpha damage)	T = [270, 1290]°C [Am] = 8.77, 18.95 at.% O/M ~ 1.99, 1.97 p = 13%, 7%
JRC-Karlsruhe	Experimental data: measurements of thermal diffusivity and specific heat capacity of different $(U,Am)O_2$ samples	T = [260, 1280]°C [Am] = 1, 5, 10, 20 at.% O/M ~ 2.00 p = 14%, 13%, 7%, 11%

Model for (U,Pu,Am)O$_{2-x}$

Building on the model for minor actinide-bearing MOX fuels published in [15] as a starting point, the effect of the Am content on the thermal conductivity is re-evaluated based on the additional recent data, which allow the extension of the model up to 15% Am. The dependencies on Pu content, deviation from stoichiometry and porosity are kept as in [15]. A modelling step forward is here represented by an advanced description of the irradiation effects following the approach published by Lucuta et al. [39], which is also applied to the thermal conductivity of the U-Am-O system (next sub-section). The achieved model reads as follows:

$$\mathrm{k_0(T, x, [Pu], [Am], p)} = \left(\frac{1}{\mathrm{A + BT + Q_{bu}(bu)}} + \frac{\mathrm{D}}{\mathrm{T^2}}\mathrm{e}^{-\frac{\mathrm{E}}{\mathrm{T}}}\right)(1-\mathrm{p})^{2.5} \quad (8)$$

$$\mathrm{k(T, x, [Pu], [Am], p, bu) = R_{dmg}(bu, T) \cdot k_0 - G_{bu}(bu)} \quad (9)$$

with $\mathrm{A = A_0 + A_x \cdot x + A_{Pu}[Pu] + A_{Am}[Am]}$ and $\mathrm{B = B_0 + B_{Pu}[Pu] + B_{Am}[Am]}$, while the k_0 formulation (coherent with Eq. 6) is already corrected with an additional term $\mathrm{Q_{bu}(bu)} = 3 \cdot 10^{-6}\mathrm{bu}^2 + 4 \cdot 10^{-4}\mathrm{bu}$ (null if the burnup is null) as a way to account for the non-recovery of lattice damages at low irradiation temperatures (indeed it contributes to the degradation of the lattice vibration contribution to the thermal conductivity).

The effects of irradiation on the (U,Pu,Am)O$_{2-x}$ thermal conductivity are also represented by R_{dmg} (Lucuta-style factor modelling the impact of defect annealing via irradiation temperature, less effective while the burnup increases [30, 39]) and G_{bu} (burnup degradation term supported by recently available data [30]), expressed as follows:

$$\mathrm{R_{dmg}(bu, T)} = 1 - \frac{0.053 \cdot \mathrm{bu}}{1 + \exp\left(\frac{\mathrm{T - T_d}}{\Delta \mathrm{T_d}}\right)} \quad (10)$$

where $\mathrm{T_d}$ (K) $= -3.39 \cdot \mathrm{bu} + 1043$ and $\Delta\mathrm{T_d}$ (K) $= 1.8 \cdot \mathrm{bu} + 30.5$

$$\mathrm{G_{bu}(bu)} = 2 \cdot 10^{-5}\mathrm{bu}^2 + 4 \cdot 10^{-3}\mathrm{bu} \quad (11)$$

The proposed model formulation is statistically-assessed based on the regressor p-values (< 5%), which confirms that it is supported by the fitting dataset considered in this work. While the coefficients inside the terms Q_{bu}, R_{dmg} and G_{bu} are already provided in the above equations, with their best-estimate values as calibrated on the data, the other model regressors and associated standard errors are collected and detailed in Table 5.

Table 5: Results of the best fit of the statistically-assessed correlation for the thermal conductivity of $(U,Pu,Am)O_{2-x}$ (Eq. 8 – k_0 regressors).

Regressor	Units	Estimate	Std. Error
A_0	m K W^{-1}	1.926 10^{-2}	*
A_{Pu}	m K W^{-1}	2.63 10^{-8}	*
A_{Am}	m K W^{-1}	0.6457	0.02733
A_x	m K W^{-1}	1.06 10^{-6}	*
B_0	m W^{-1}	2.39 10^{-4}	*
B_{Pu}	m W^{-1}	1.37 10^{-13}	*
B_{Am}	m W^{-1}	1.151 10^{-4}	4.355 10^{-5}
D	W K m^{-1}	5.27 10^{9}	*
E	K	1.711 10^{4}	*

* Values of regressor estimates and associated standard errors (at least one order of magnitude lower compared to the estimates) are in line with those published in [15].

Some graphical representations of the model behaviour and its verification against the fitted data are provided in Figure 3. The model applicability can be recommended over the entire temperature range up to fuel melting (although the majority of the data pertains to the low temperature range < 1800 K), Pu content up to 35 at.%, Am contents up to 15 at.%, O/M ratio from 2.00 (stoichiometry) down to 1.97, porosity up to 12% and burnup up to 80 GWd/t.

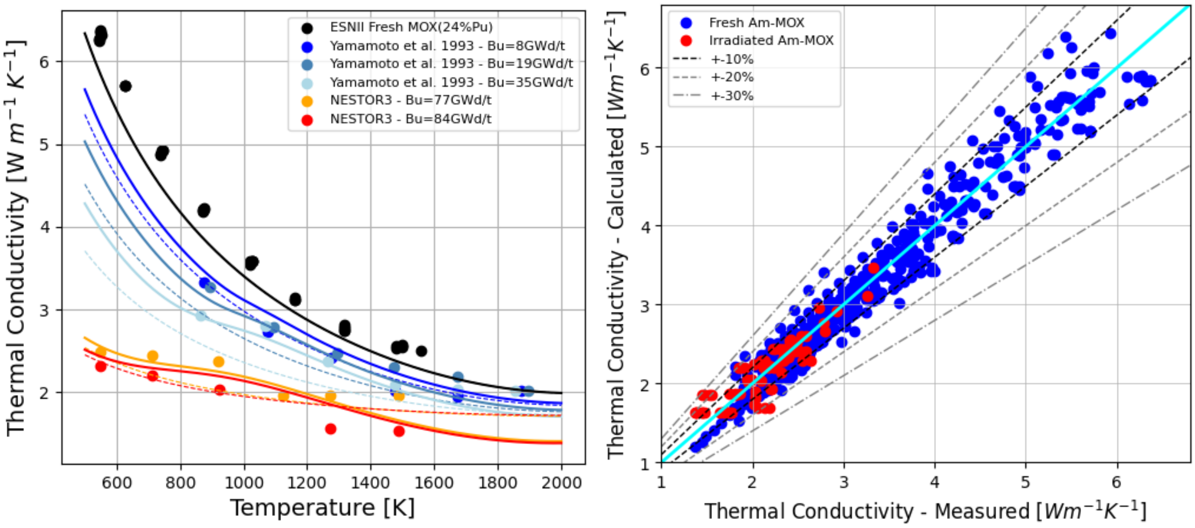

Figure 3: Left: Comparison of the novel model proposed for the thermal conductivity of $(U,Pu,Am)O_{2-x}$ (full lines) and of the model already published in [15] (dashed lines), as a function of temperature, in comparison with experimental data on irradiated fuels. Right: Comparison of the model predictions with the data considered.

Model for $(U,Am)O_{2-x}$

For what concerns the modelling of $(U,Am)O_2$ thermal conductivity, the approach adopted closely follows the theoretical basis of solid-state physics, particularly for what concerns the lattice vibration contribution. Coefficients A and B, describing the phonon-lattice thermal resistivity and the intrinsic lattice thermal resistivity, respectively, are no more assumed as linearly dependent on the variables of interest (Am content and O/M, in this case), as in the majority of literature works (e.g., [38, 40]).

Nevertheless, a more theoretically-grounded approach has been adopted by Fukushima et al. [35], which is here retained and tailored on the currently available dataset.

The lattice defect thermal resistivity A of dielectric solids can be expressed by the following equation, re-arranged in the $(U,Am)O_{2-x}$ in the sum of two terms, i.e., W0 and W1 depending on the concentration of Am considered as a solute in the UO_2 lattice:

$$A = \frac{\pi^2 \overline{V} \theta}{3 v^2 h} \sum \Gamma_i = W_0 + W_1([Am])$$

where $\overline{V}$ is the average atomic volume, θ the Debye temperature, v the average phonon velocity, h the Planck constant, Γ_i the scattering cross-section of phonons by the point defect i. W_0 is the contribution to lattice thermal resistivity caused by the defects (such as or caused by impurities) included in the solid solution and is considered to be very close to that of the solvent lattice (UO_2). $W_1([Am])$ is the additional thermal resistivity caused by the interaction of phonons with solutes (Fukushima et al. describe this referring to Nd, Sm, Eu, Y solute in the UO_2 solvent matrix). Both W_0 and W_1 can be considered as model parameters to be fitted on a dataset for the system of interest.

Based on literature on multi-valence states in the uranium oxide matrix (e.g., [41]), the chemical formulation of the system determined by the Am solute in the UO_2 solvent is $(U^{4+}_{1-2x}; U^{5+}_{x}; R^{3+}_{x})O^{2-}_{2}$. Hence:

$$\sum_i \Gamma_i = \Gamma_{U4+} + \Gamma_{U5+} + \Gamma_{Am3+} = [C_i]\left\{(\frac{M_{mean} - M_i}{M_{mean}})^2 + \varepsilon(\frac{r_{mean} - r_i}{r_{mean}})^2\right\} =$$

$$= [Am](1-[Am])(\frac{M_U - M_{Am}}{M_{mean}})^2 + \varepsilon\Big[[Am](1-[Am])(\frac{r_{U4} - r_{U5}}{r_{mean}})^2 + 2[Am]^2\left(\frac{r_{U4} - r_{U5}}{r_{mean}}\right)\left(\frac{r_{Am3} - r_{U4}}{r_{mean}}\right) + [Am](1-[Am])(\frac{r_{Am3} - r_{U5}}{r_{mean}})^2\Big]$$

$$\simeq [Am](1-[Am])\left\{(\frac{M_U - M_{Am}}{M_{mean}})^2 + \varepsilon\left[\left((\frac{r_{U4} - r_{U5}}{r_{mean}})^2 + (\frac{r_{Am3} - r_{U5}}{r_{mean}})^2\right)\right]\right\}$$

where $[C_i]$ is the concentration of the element I, M the atomic mass, r the ionic radius, and ε the strain generated in the lattice by the inclusion of the solute. Furthermore, we $M_{mean} = [Am]M_{Am} + (1-[Am])M_U$ and $r_{mean} = [Am]r_{Am3} + [Am]r_{U5} + (1-2[Am])r_{U4}$. The formulation agrees also with [42], indicating that the degradation of the lattice thermal conductivity due to impurities should express the proportionality to their concentration, and to the square of the mass difference of the impurity compared to U [35], [42]. Since $[Am] \gg [Am]^2$, the model for A is further simplified as follows:

$$A = W_0 + W_1[Am]\left\{(\frac{M_U - M_{Am}}{M_{mean}})^2 + \varepsilon\left[\left((\frac{r_{U4} - r_{U5}}{r_{mean}})^2 + (\frac{r_{Am3} - r_{U5}}{r_{mean}})^2\right)\right]\right\}$$

For what concerns the strain field parameter ε, it is generally evaluated by fitting dedicated experimental data. Middleburg et al [43] estimated changes in volume of the uranium dioxide lattice due to the accommodation of soluble fuel additives and fission products by means of simulations based on empirical inter-atomic potentials, while Fukushima et al. [35] inferred values for the solid solutions $(U,Nd)O_2$, $(U,Sm)O_2$, $(U,Eu)O_2$.from thermal conductivity measurements. By relying on these data and the ionic radii of the involved elements, a value $\varepsilon = 103$ is extrapolated for the stoichiometric $(U,Am)O_2$ system. The O/M ratio is currently not present in the formula for A due to the small amount of data on $(U,Am)O_{2-x}$ available. The effect of oxygen on the phonon-lattice scattering corresponds to a contribution to the strain field of the matrix, while the absence of oxygen atoms generates a variation of the valence state of cations and leads to changes in the ionic radii of these elements.

The intrinsic lattice resistivity B is widely expressed in literature (e.g., in [28-33], [25, 26, 35, 44]) according to the Liebfried-Schlomann relationship:

$$B = \frac{\gamma^2}{\left(\frac{24}{10}\right) 4^{\frac{1}{3}} (\frac{h}{k})^3 \bar{M}\bar{V}^{\frac{1}{3}}\, \theta_D^{\frac{1}{3}}}$$

where $\bar{V}$ is the average atomic volume, $\bar{M}$ the average atomic mass, θ the Debye temperature, h the Planck constant, k the Boltzmann constant, γ the Gruneisen constant. In line with previous authors, the B term can be re-written, assuming the Gruneisen constant similar for $(U,Am)O_2$ and UO_2, in the following way:

$$B = W_2 \left(\frac{M_{SS}}{M_{UO2}}\right)^{\frac{1}{2}} \left(\frac{a_{SS}}{a_{UO2}}\right)^2 \left(\frac{T_{M,UO2}}{T_{M,SS}}\right)^{\frac{3}{2}} \left(\frac{\gamma_{SS}}{\gamma_{UO2}}\right) \cong W_2 \left(\frac{M_{SS}}{M_{UO2}}\right)^{\frac{1}{2}} \left(\frac{a_{SS}(T)}{a_{UO2}(T)}\right)^2 \left(\frac{T_{m,UO2}}{T_{m,SS}([Am], O/M)}\right)^{\frac{3}{2}}$$

where W_2 is a fitting parameter, and the subscript SS means Solid Solution, i.e., the $(U,Am)O_2$ system of interest. Hence, $T_{m,SS}([Am], O/M)$ is modelled according to the novel correlation for $(U,Am)O_2$ (Eq. 5, Table 3). $a_{SS}(T)$ is the lattice parameter of the solid solution, evaluated as $a_{SS}[\dot{A}] = a_{UO2} * (1 - Am]) + a_{AmO2} * [Am]$, with a_{UO2} and a_{AmO2} according to [10, 45] and [44, 46] , respectively.

The outlined models for A and B are introduced in a physically-grounded formulation of the thermal conductivity of fresh $(U,Am)O_2$, reading:

$$k_0(T, [Am], p) = \left(\frac{1}{A + BT} + \frac{D}{T^2} e^{-\frac{E}{T}}\right)\left(\frac{1 - p}{1 + 0.5p}\right) \qquad (12)$$

where the porosity effect is modelled via the Maxwell-Eucken correction factor for spherical pores, which proves to better describe the available data on $(U,Am)O_2$ compared to the modified Loeb factor used in [15] for minor-actinide MOX and also (coherently) in the newly proposed model for $(U,Pu,Am)O_{2-x}$ (Eq. 8). The values of the model regressors and associated standard errors, resulting from the best fit and statistical analysis of the dataset, are collected and detailed in Table 6.

Table 6: Results of the best fit of the statistically-assessed correlation for the thermal conductivity of $(U,Am)O_2$ (Eq. 12).

Regressor	Units	Estimate	Std. Error
W_0	$m\ K\ W^{-1}$	$7.011\ 10^{-2}$	$4.944\ 10^{-3}$
W_1	$m\ K\ W^{-1}\ at./^{-1}$	$7.017\ 10^{-2}$	$3.153\ 10^{-3}$
W_2	$m\ W^{-1}$	$2.010\ 10^{-4}$	$6.099\ 10^{-6}$
D	$W\ K\ m^{-1}$	$1.66\ 10^{10}$	$9.641\ 10^{9}$
E	K	$2.072\ 10^{4}$	$1.548\ 10^{3}$

For what concerns the behaviour of U-Am-O thermal conductivity fuel under irradiation, no dedicated data are available in literature / accessible by the authors at the moment. Nevertheless, a contribution to thermal conductivity degradation can be represented, associated with self-irradiation, i.e., the α-decay of Am and resulting defects in the fuel material lattice. This is represented via a Lucuta-style factor, expressing the effective recovery of the self-irradiation at sufficiently high temperature, while the thermal conductivity at low temperatures is lowered. This is modelled as follows:

$$k_{self-irr}(T,[Am],p) = R_{dmg}([Am],T) \cdot k_0 \tag{13}$$

$$R_{dmg}([Am],T) = 1 - \frac{H \cdot [Am]}{1 + \exp\left(\frac{T - T_d}{\Delta T_d}\right)} \tag{14}$$

where T_d (K) $= 600 - 2000([Am] - 0.2)$, ΔT_d (K) $= 80 + 1000([Am] - 0.1)$ and H = 2.20511.

This modelling applies to a fuel condition at which the defect concentration has reached the saturation level, since it does not consider the accumulation of defects prior to saturation. Nevertheless, damage saturation is supposed to occur in just a few weeks, depending on the Am content. A showcase of the model behaviour, including the comparison with the reference (available) data, is provided in Figure 4. The model applicability can be recommended over the entire temperature range up to fuel melting (although the data pertain to the low temperature range < 1550 K), Am contents up to 20 at.%, O/M ratio from 2.00 (stoichiometry) down to 1.97, porosity up to 14%.

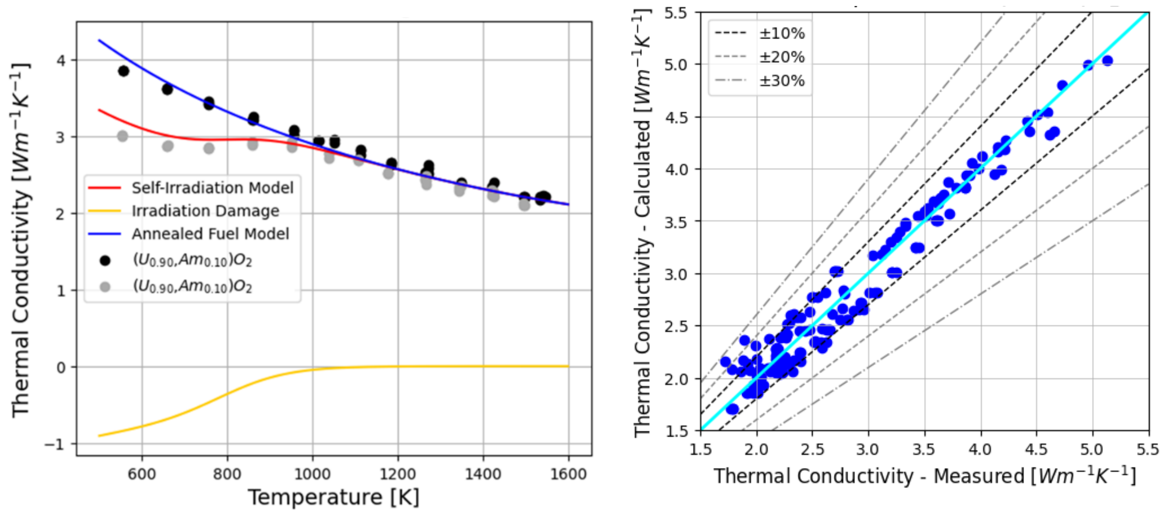

Figure 4: Left: Behaviour of the novel model proposed for the thermal conductivity of $(U,Am)O_2$, as a function of temperature, in comparison with experimental data at 10% Am. Right: Comparison of the model predictions with the data considered.

2.3 Specific heat modelling

A first modelling development has been performed within the PATRICIA Project, accounting for the open literature available up to 2021 [47]. The model formulation is physically-grounded since based on solid-state physics theory, and it is fitted on experimental data available for U-Pu MOX and heterogeneous $(U,Pu,Am)O_2$ (i.e., with Am contents > 10%). The result is a model that represents well the specific heat capacity of Am-MOX fuels at those compositions for which data are available, but that needs to be extrapolated to high temperatures close to fuel melting (due to the lack of experimental data at high temperatures, that are difficult to be measured), to Am contents < 5% or to $(U,Am)O_2$ compositions, still providing reasonable results. This is model is called *"Exponential"* in the following.

Moreover, a first trial to describe the Bredig transition at high temperature for U-Pu MOX fuels has been achieved, on the basis of available data from atomic-scale computations [48], by adding a Gaussian-like function peaked at high temperatures to the model. The shift at lower temperatures of the Bredig transition peak with an increasing Pu content is also represented by the model. This model is called *"Bredig transition"* in the following.

The *"Exponential"* model is dominated by exponential-like terms, and it is defined as follows:

$$c_p(T,[Pu],[Am]) = \frac{C_1 \Theta^2 e^{\Theta/T}}{T^2(e^{\Theta/T}-1)^2} + 2C_2T + \frac{C_3 E_a e^{-E_a/T}}{T^2} \tag{15}$$

The generic model regressor, except for C_1, is expressed as $X = X_0 + X_{Pu}\cdot[Pu] + X_{Am}\cdot[Am]$, where X indicates C_2, C_3, Θ, E_a. The associated coefficient values, derived from a best-fit of the available data [47], are collected in Table 7.

Table 7: Results of the best fit of the *"Exponential"* correlation for the specific heat capacity of $(U,Pu,Am)O_{2-x}$ (Eq. 15)

Regressor	Units	Estimate
C_1	J mol^{-1}K^{-1}	85.008
ϑ_0	K	596.045
ϑ_{Pu}	K	−39.431
ϑ_{Am}	K	197.02
$C_{2,0}$	J mol^{-1} K^{-2}	$1.253\cdot10^{-3}$
$C_{2,Pu}$	J mol^{-1} K^{-2}	$1.456\cdot10^{-2}$
$C_{2,Am}$	J mol^{-1} K^{-2}	$1.226\cdot10^{-3}$
$C_{3,0}$	J mol^{-1}	$1.208\cdot10^{7}$
$C_{3,Pu}$	J mol^{-1}	$1.147\cdot10^{7}$
$C_{3,Am}$	J mol^{-1}	$2.653\cdot10^{7}$
$E_{a,0}$	K	15969.1
$E_{a,Pu}$	K	7996.53
$E_{a,Am}$	K	4360.34

The ranges of applicability of the model are the following: T = [300, $T_{melting}$] K, [Pu] = [0, 40] at.%, [Am] = [0, 70] at.%, O/M = [1.93 – 2.02].

The *"Bredig transition"* model adds a gaussian-like term to the *"Exponential"* model of Eq. 15, hence it is defined as follows:

$$c_p(T,[Pu]) = \frac{C_1 \Theta^2 e^{\Theta/T}}{T^2(e^{\Theta/T}-1)^2} + 2C_2T + \frac{C_3 E_a e^{-E_a/T}}{T^2} + He^{-\frac{(T-T_{BT})^2}{W}} \tag{16}$$

The generic model regressor, except for C_1, is expressed as $X = X_0 + X_{Pu}\cdot[Pu]$, where X indicates C_2, C_3, Θ, E_a, H, T_{BT}, W. The associated coefficient values, derived from a best-fit of the available data [47] (concerning just U-Pu MOX [48], hence not allowing an explicit dependence on the Am content), are collected in Table 8.

Table 8: Results of the best fit of the *"Bredig transition"* correlation for the specific heat capacity of $(U,Pu)O_{2-x}$ (Eq. 16).

Regressor	Units	Estimate
C_1	J mol^{-1} K^{-1}	79.887
ϑ_0	K	552.907
ϑ_{Pu}	K	−66.296
$C_{2,0}$	J mol^{-1} K^{-2}	$7.171\cdot10^{-3}$
$C_{2,Pu}$	J mol^{-1} K^{-2}	$5.113\cdot10^{-3}$
$C_{3,0}$	J mol^{-1}	$3.407\cdot10^{6}$
$C_{3,Pu}$	J mol^{-1}	$-6.031\cdot10^{6}$
$E_{a,0}$	K	18772.168
$E_{a,Pu}$	K	−220.457
H_0	J mol^{-1} K^{-1}	37.869
H_{Pu}	J mol^{-1} K^{-1}	6.667
$T_{BT,0}$	K	2622.932
$T_{BT,Pu}$	K	−265.822
W_0	K	33176.287
W_{Pu}	K	−17626.931

The ranges of applicability of the model are the following: T = [300, $T_{melting}$] K, [Pu] = [0, 100] at.%, O/M = [1.95, 2.02].

The two models have been implemented in an extended version of TRANSURANUS v1m4j22 and tested against the transient scenarios (Beam Power Jump) of concern for the sub-critical core configuration of MYRRHA targeted within PATRICIA. The effect on the pin performance results proved to be limited, especially due to the too fast dynamics of the transient (+70% of linear power in 3 s) and to the limited operational temperature of the MYRRHA fuel, at which different specific heat models are aligned with each other.

The achievement of additional CALPHAD-based / atomic-scale data from the Work Package 4 of the PATRICIA Project [19, 49] enabled a re-consideration of the specific heat modelling for fuel performance codes, broadening the fuel material options to be considered, i.e., heterogeneous $(U,Am)O_{2-x}$ blanket-type fuel in addition to homogeneous $(U,Pu,Am)O_{2-x}$ driver-type fuels. The results of this modelling activity are described in what follows. The basic structure of the model is kept the same as the physically-grounded one previously recalled (Eq. 15, in line with Fink's model [50] highly recommended for UO_2 and PuO_2). The strategy adopted now distinguishes between $(U,Pu,Am)O_{2-x}$ and $(U,Am)O_{2-x}$ systems, on the basis of a data analysis, and considers both experimental and computational data in the low temperature regime, where data of different nature are coherent. At high temperature instead, for the $(U,Am)O_{2-x}$ system, two model developments have been performed: one considers just experimental data, while the other considers the Bredig transition indicated by the novel PATRICIA data on $(U,Am)O_{2-x}$ [19, 49]. Hence, the model based on experimental data at high temperature keeps the exponential-like form and it is called *"Exponential"* in what follows, while the model built on computational data at high temperature is gaussian-like (to represent the Bredig transition) and it is called *"Bredig transition"* in the following. A collection of the data composing the fitting dataset, for both the U-Pu-Am-O and U-Am-O systems and including both experimental (from adiabatic calorimetry / drop calorimetry / heat flux Differential Scanning Calorimetry / laser flash / direct heating pulse) and computational (CALPHAD / atomic-scale) data is provided in Table 9.

Table 9: Datasets considered for the modelling of specific heat capacity of Am-bearing oxide fuels, extending the database already considered in [47].

$(U,Pu,Am)O_{2-x}$		
Reference	**Details**	**Ranges covered**
Valu et al. 2014 [51] Pavlov et al. 2017 [42] Ronchi et al. 1999 [36] + older	Experimental data on UO_2 (sim-fuel data on as-irradiated UO_2 from Lucuta 1996 [39])	T = [25, 2700]°C (bu = 22.5, 60 GWd/t)
Oetting et al. 1982 [52] + older	Experimental data on PuO_2	T = [25, 2100]°C
Kandan et al. 2004, 2008 [53, 54] Rao et al. 2006, Harding et al. 1989 [55] + older	Experimental data on $(U,Pu)O_{2-x}$	T = [25, 2700]°C for [Pu] = [20, 25] at.% T = [25, 1500]°C for [Pu] = [25, 65] at.% O/M = [1.92, 2.00]
PATRICIA WP4	CALPHAD results on $(U,Pu,Am)O_{2-x}$	T = [250, 2700]°C [Pu] = 30 at.% [Am] = [1, 5] at.% O/M = [1.97, 2.00]
$(U,Am)O_{2-x}$		
Reference	**Details**	**Ranges covered**
Valu et al. 2014 [51] [] Pavlov et al. 2017 [42] Ronchi et al. 1999 [36] + older	Experimental data on UO_2 (sim-fuel data on as-irradiated UO_2 from Lucuta 1996 [39])	T = [25, 2700]°C (bu = 22.5, 60 GWd/t)
Valu et al. 2014 [51] [] Epifano et al. 2017 [56]	Experimental data on $(U,Am)O_{2-x}$	T = [25, 1500]°C [Am] = [8.77, 68] at.% O/M = [1.87, 2.00]
PATRICIA WP4	CALPHAD results on $(U,Am)O_{2-x}$	T = [250, 2700]°C [Am] = [10, 20] at.% O/M = [1.93, 1.95]
Labonne et al. 2023 [19], [19, 49]	Atomic-scale data on UO_2	T = [1200, 2700]°C
Labonne et al. 2023 [19], [19, 49]	Atomic-scale data on $(U,Am)O_2$	T = [1200, 2700]°C [Am] = [5, 50] at.%

"Exponential" models for $(U,Pu,Am)O_{2-x}$ and $(U,Am)O_{2-x}$

The *"Exponential"* model, in line with Eq. 15, reads:

$$c_p(T, [Pu], [Am]) = \frac{C_1 \Theta^2 e^{\Theta/T}}{T^2 (e^{\Theta/T} - 1)^2} + 2C_2 T + \frac{C_3 E_a e^{-E_a/T}}{T^2} \tag{17}$$

The generic model regressor, except for C_1, is expressed as $X = X_0 + X_{Pu} \cdot [Pu] + X_{Am} \cdot [Am]$, where X indicates C_2, C_3, Θ, E_a. The coefficient values and associated standard errors, derived from a best-fit of the available data [33], are collected in Table 10 for the $(U,Pu,Am)O_{2-x}$ system, while in Table 11 for the $(U,Am)O_{2-x}$ system.

Table 10: Results of the updated best-fit of the *"Exponential"* correlation (Eq. 17) for the specific heat capacity of $(U,Pu,Am)O_{2-x}$.

Regressor	Units	Estimate	Std. Error
C_1	$J\ mol^{-1}\ K^{-1}$	81.18	$7.23\cdot10^{-1}$
ϑ_0	K	527.6	16.2
ϑ_{Pu}	K	−12.26	22.5
ϑ_{Am}	K	3460	$6.037\cdot10^{2}$
$C_{2,0}$	$J\ mol^{-1}\ K^{-2}$	$1.809\cdot10^{-3}$	$3.159\cdot10^{-4}$
$C_{2,Pu}$	$J\ mol^{-1}\ K^{-2}$	$6.435\cdot10^{-3}$	$3.058\cdot10^{-4}$
$C_{2,Am}$	$J\ mol^{-1}\ K^{-2}$	$1.446\cdot10^{-2}$	$2.726\cdot10^{-3}$
$C_{3,0}$	$J\ mol^{-1}$	$7.247\cdot10^{6}$	$3.306\cdot10^{5}$
$C_{3,Pu}$	$J\ mol^{-1}$	$-1.219\cdot10^{7}$	$7.67\cdot10^{6}$
$C_{3,Am}$	$J\ mol^{-1}$	$-1.858\cdot10^{7}$	$4.648\cdot10^{6}$
$E_{a,0}$	K	14460	$1.866\cdot10^{2}$
$E_{a,Pu}$	K	1061	$1.872\cdot10^{2}$
$E_{a,Am}$	K	−2092	$6.25\cdot10^{3}$

Table 11: Results of the updated best-fit of the *"Exponential"* correlation (Eq. 17) for the specific heat capacity of $(U,Am)O_{2-x}$.

Regressor	Units	Estimate	Std. Error
C_1	$J\ mol^{-1}\ K^{-1}$	81.15	1.62
ϑ_0	K	521.10	35.43
ϑ_{Am}	K	220.4	39.6
$C_{2,0}$	$J\ mol^{-1}\ K^{-2}$	$2.009\cdot10^{-3}$	$6.2\cdot10^{-4}$
$C_{2,Am}$	$J\ mol^{-1}\ K^{-2}$	$4.59\cdot10^{-3}$	$5.44\cdot10^{-4}$
$C_{3,0}$	$J\ mol^{-1}$	$6.494\cdot10^{6}$	$5.54\cdot10^{4}$
$C_{3,Am}$	$J\ mol^{-1}$	$-3.747\cdot10^{6}$	$4.65\cdot10^{6}$
$E_{a,0}$	K	14270	331
$E_{a,Am}$	K	10660	$2.74\cdot10^{3}$

While the model for $(U,Pu,Am)O_{2-x}$ can be applied in the same ranges associated to Eq. 15 [47], the novel model specific for $(U,Am)O_{2-x}$ is applicable up to an Am content of 50 at.%, in the entire temperature range from room temperature up to fuel melting temperature. The effect of the Am content and of the fuel O/M on the specific heat prove secondary for the moment (in the ranges where data are currently available) compared to the temperature and Pu content ones, but more data on e.g., hypo-stoichiometric fuels would be required to better assess the O/M impact. For the moment, given the irrelevance of the O/M on the specific heat capacity in the ranges where data are available, i.e., [1.97, 2.00] for the U-Pu-Am-O system and [1.93, 1.95] for the U-Am-O system, the outlined model for U-Am-O is deemed applicable also to stoichiometric fuel compositions. No data are currently available about a potential effect of the fuel burnup on the specific heat capacity.

The behaviour of both "*Exponential*" models is showcased in Figure 5. The specific heat capacity values provided by the novel models at high temperatures are dictated by the recent CALPHAD data achieved by PATRICIA WP4, and transferred to WP5 to support the modelling activity.

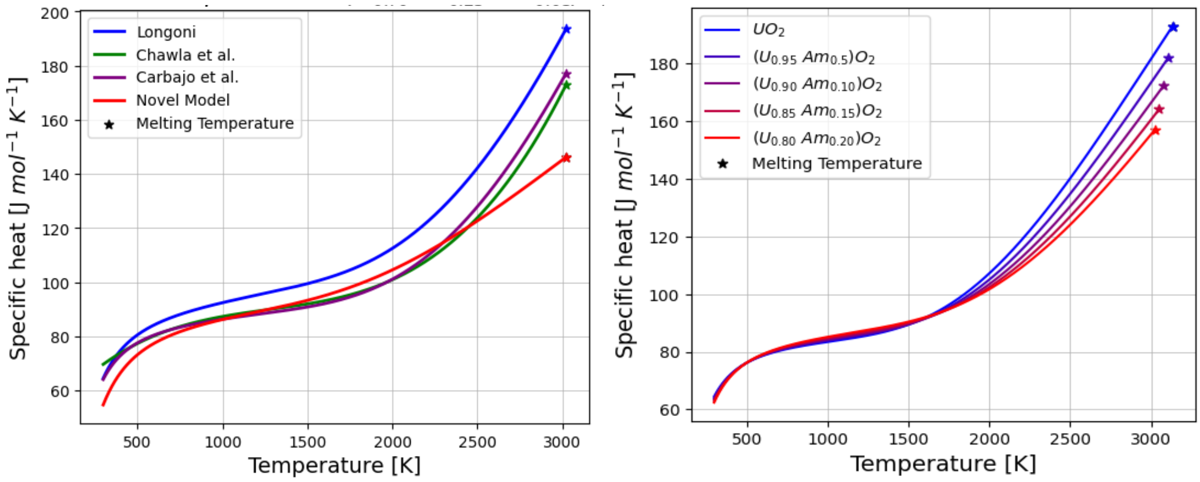

Figure 5: Left: Behaviour of the novel model proposed for the specific heat capacity of (U,Pu,Am)O_2, as a function of temperature, for 25% Pu and 5% Am contents, in comparison with already existing literature models. Right: Behaviour of the novel model proposed for the specific heat capacity of (U,Am)O_2, as a function of temperature, for different relevant Am contents.

"Bredig transition" model for (U,Am)O_2

To account for the Bredig Transition, the exponential trend at high temperatures has been substituted by a Gaussian-like term able to describe the behaviour of the specific heat capacity of (U,Am)O_2 predicted by atomic-scale calculations in the high-temperature region. It is important to account for atomic-scale indications about the behaviour of thermo-physical properties at high temperature given the difficulties (and associated uncertainties) to perform measurements in the temperature region close to fuel melting, where available experimental data suffer from significant scattering. The novel data from PATRICIA WP4 [19, 49] enabled the introduction of an explicit dependence on the fuel Am content, which proves anyway limited compared to the temperature and Pu content dependences. The O/M effect is not represented by the atomic-scale data currently achieved and considered [19].

The model is defined as follows:

$$c_p(T, [Pu], [Am]) = \frac{C_1 \Theta^2 e^{\Theta/T}}{T^2 (e^{\Theta/T} - 1)^2} + 2C_2 T + He^{-\frac{(T - T_{BT})^2}{W}} \tag{18}$$

The generic parameter, except for C1, is expressed as $X = X_0 + X_{Am} \cdot [Am]$, where X indicates C_2, Θ, E_a, H, T_{BT}, W. The coefficient values and associated standard errors, derived from a best-fit of the available data, are collected in Table 12.

Table 12: Results of the updated best-fit of the *"Bredig transition"* correlation (Eq. 18) for the specific heat capacity of $(U,Am)O_2$.

Regressor	Units	Estimate	Std. Error
C_1	$J\ mol^{-1}\ K^{-1}$	80.08	0.58
ϑ_0	K	548.7	14.7
ϑ_{Am}	K	−48.43	61.52
$C_{2,0}$	$J\ mol^{-1}\ K^{-2}$	$3.215 \cdot 10^{-3}$	$2.025 \cdot 10^{-4}$
$C_{2,Am}$	$J\ mol^{-1}\ K^{-2}$	$3.102 \cdot 10^{-3}$	$2.912 \cdot 10^{-4}$
H_0	$J\ mol^{-1}\ K^{-1}$	38.99	0.72
H_{Am}	$J\ mol^{-1}\ K^{-1}$	−86.77	2.45
$T_{BT,0}$	K	2661	4.61
$T_{BT,Am}$	K	−999.7	38.2
W_0	K	84490	$4.52 \cdot 10^{3}$
W_{Am}	K	−12110	$2.651 \cdot 10^{4}$

The behaviour of the novel "Bredig transition" model is showcased in Figure 6. Although the U-Am-O (atomic-scale) data showing the Bredig transition at high temperatures currently cover the range Am = [0, 50] at.% and refer to stoichiometric fuel (O/M = 2.00) [19], [19, 49], the model applicability is for the moment recommended for Am contents up to 20 at.%, while a negligible effect of the deviation from fuel stoichiometry can be supposed (see also Section 5.2). No data are currently available about a potential effect of the fuel burnup on the specific heat capacity. Future analyses should focus on the most extensive validation possible of the model proposed, against new data (both experimental and CALPHAD / atomic-scale) that will become available, covering e.g., the hypo-stoichiometric range and assessing the potential effect of the fuel burnup.

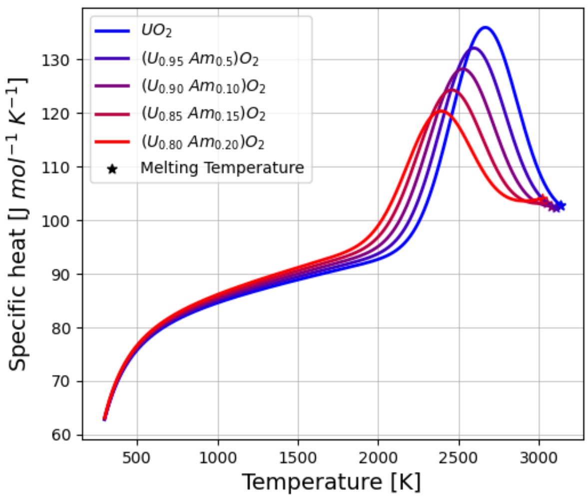

Figure 6: Behaviour of the novel model proposed for the specific heat capacity of $(U,Am)O_2$, as a function of temperature, for different Am contents up to 20%.

2.4 Creep modelling

The present model for stationary creep of standard UO_2 fuel applied in the TRANSURANUS code stems from the original work of Lassmann and Moreno in 1977 [57].The empirical correlation is based on that of steady-state creep proposed by Solomon from 1971 [57], and applied in the LIFE-1 code of ANL. Their correlation, in turn, was inferred from various compressive creep measurements both in reactor and out-of-pile, indicating that in-reactor creep has two distinct temperature regimes. Above roughly 1000°C, normal thermal creep is enhanced by fission with an apparent activation energy. Below this temperature, an athermal creep mechanism is observed that was referred to as fission-induced, since without fission no creep would occur. Within the experimental scatter, the steady-state creep rates depend linearly on stress and fission rate in both regimes:

$$\dot{\varepsilon} = A(\varphi)\sigma^{4.5}e^{-Q/_{RT}} + \frac{A_1(\varphi)\sigma}{G^2}e^{-Q/_{RT}} + B\sigma\varphi \tag{19}$$

where

$$A(\varphi) = \frac{\left(1.38\cdot10^{-4} + 1.73\cdot10^{-18}\varphi\right)}{D-90.5} \tag{20}$$

$$A_1(\varphi) = \frac{\left(9.73\cdot10^{6} + 1.22\cdot10^{-7}\varphi\right)}{D-87.7}$$

and σ stands for the effective stress, *G* represents the grain size, *D* corresponds to the fuel density (%), while φ represents the flux during the time step under consideration.

For mixed oxide fuel, there is a creep correlation for FBR MOX fuel implemented in TRANSURANUS that was proposed by Többe in 1975[58]. It is very similar to that of the European Catalogue published in the frame of the ENSII plus project in 2015 that in turn was based on the work of Matthews et al [59], but neither of them are in the open literature. In recent papers dealing with modelling PCMI, Bernard et al [60] and Portelette et al [61] and confirmed that power ramps performed on MOX fuel have shown that SCC PCI performances of MOX fuel are significantly higher than those of UO_2 fuels. It is therefore reasonable to assume that creep in MOX is higher in comparison with UO_2 fuel, as pointed out by Caillot et al [62] who showed that at temperatures about 1550°C and a stress of 40 MPa the creep strain was about a factor 2 greater in MOX compared to UO_2.

Based on the recommendation expressed in the ESNII plus report, one should assess the old creep correlations for MOX, and in particular consider the work of Malygin et al. [63-65], who published data on the creep of both UO_2 and MOX fuels, and took into considerations details of the point defects. A first version of this semi-mechanistic creep model for MOX fuel is implemented in the TRANSURANUS code. It takes into consideration the dependency on porosity, stress, T, flux, grain size and when necessary also point defect concentrations or deviations from stoichiometry that are typical for FBR MOX fuels.

Malygin et al reviewed experimental data and observed that

- the thermal creep for UO_2 under compression is a linear function of the stress below 30-40 MPa, while a power-law dependence with an exponent of 4-5 is observed for higher pressures.

- In the linear range, the creep rate is inversely proportional with the squared grain size.
- The activation energy of the thermal creep is close to that of uranium diffusion by means of a vacancy mechanism

The first two observations are very consistent with those of Solomon et al. [57]. On the basis of these, together with the third observation, Malygin et al. [63] concluded that at low stress, creep is controlled by the diffusion mechanism and at high stress by dislocation climb, and that both processes operate in parallel and are linearly dependent on the diffusion coefficient. They proposed an exponent for the stress equal to 1 in the stress range 10-30 MPa and 4.5 for stresses above 40 MPa.

The thermal creep is thus also dependent on the diffusion coefficient, which is controlled by that of uranium in the ionic compound. Malygin and his co-workers [64, 65] proposed an expression of this diffusion coefficient that takes into account the effect of stoichiometry deviations. For this purpose, they defined the classical defects (Frenkel, Schottky) and made use of the corresponding mass action laws. They ended up with a formulation for the thermal creep rate of UO_2 that depends on the Temperature (T), stress (σ), grain size (G), porosity (P) and deviation from stoichiometry (x):

$$\dot{\varepsilon}_{th,UO2} = \left(1+0.3P^{1.8}\right) f\left(x,T\right)\left[\frac{A\sigma}{G^2} + B\sigma^{4.5} e^{-0.5/k_B T}\right] \tag{21}$$

where

$$f\left(x,T\right) = \frac{e^{-1.9/k_B T}\left[\sqrt{x^2 + 123 e^{-2.1/k_B T}} + x\right]^2}{1+4\cdot 10^3 x} \tag{22}$$

and k_B represents Boltzmann constant, and the additional activation energy in the second term of the creep rate is related to the energy of interaction between a point defect and the dislocation during dislocation climb and is estimated to be 0.5 eV [64]. Malygin et al claim that after fitting the coefficient with a statistical program, their expression for thermal creep of UO_2 provides values that are 10 times in better agreement with experimental data in comparison with the MATPRO correlation from 1995, which was applied in a recent study by Safari et al [66] who also considered the effect of stoichiometry increases in WWER1000 fuel. Nevertheless, Klouzal and Matocha [67] carried out their own fitting of the equation proposed by Magylin et al and found slightly different coefficients, which are still within the limits of the intervals proposed by Malygin et al. [64].

The correlation for UO_2 also contains the irradiation induced creep rate proposed by Malygin et al in 2010 [65]. Their analysis of data showed that this component of stationary creep is directly proportional with the applied stress and fission density, independent of the grain size, and constant below 400-500ºC but increasing with temperature beyond that range. They therefore proposed two components of irradiation induced creep. The athermal component is controlled by the blocking of interstitial atoms by dislocations and is expressed as

$$\dot{\varepsilon}_{irr1,UO2} = \frac{\sigma K\left(T,\varphi\right)}{E\left(T\right)} \tag{23}$$

where K is the rate of formation of point defects associated with displacement cascades, and E represents the elastic modulus. Malygin et al [65] solve a differential equation to describe the dynamics of the change of the concentration of trapping centers and ultimately propose the stationary solution for the formation rate of mobile radiation defects per unit volume:

$$K_{Vs}\left(T,\varphi\right)=\frac{\varphi}{\left[1+\dfrac{10^{-18}\varphi}{10^{-20}\varphi+\lambda\left(T\right)}\right]} \tag{24}$$

where the rate at which defects are freed from trapping centers can be expressed as

$$\lambda\left(T\right)=10^{11}e^{-4.5/k_BT} \tag{25}$$

For temperatures below 900°C, Malygin et al adopt the following approximation:

$$K_{Vs}\left(T,\varphi\right)=\frac{\varphi}{101} \tag{26}$$

The thermal component of the irradiation-induced creep of oxide fuel is related to the diffusion of point defects towards dislocations loops or clusters, whose orientation depends on the stress state and has the form:

$$\dot{\varepsilon}_{irr2,UO2}=A\sigma\sqrt{K}e^{-\Delta H_m/2k_BT} \tag{27}$$

where A is a constant and the square root dependency on K is because of its influence on the radiation-enhanced diffusion coefficient. Finally, the resulting formula for the stationary creep rate in UO_2 fuel combines the thermal, irradiation enhanced and irradiation-induced components.

In their paper about irradiation-induced creep of oxide fuel [65] as well as in a specific paper for the thermal creep of MOX fuel [63], Malygin and his co-workers also proposed a semi-mechanistic model for MOX fuel. The irradiation induced components have the same form as for UO_2 fuel, albeit with different parameters, and don't depend on the Pu content:

$$\dot{\varepsilon}_{irr,MOX}=\left(1+0.3P^{1.8}\right)\left(\frac{A_1\sigma K_{Vs}\left(T,\varphi\right)}{E\left(T\right)}+A_2\sigma\sqrt{K_{Vs}\left(T,\varphi\right)}e^{-Q/k_BT}\right) \tag{28}$$

The model for thermal creep in MOX fuel on the other hand considers all effects outlined above with somewhat adapted (fitting) coefficients, in addition to the effect of the Pu concentration and a different consideration of the porosity:

$$\dot{\varepsilon}_{th,MOX}=g\left(x,T\right)\left[\frac{A\left(P,Pu\right)\sigma}{G^2}+B\left(P,Pu\right)\sigma^{4.5}e^{-Q_1/k_BT}\right] \tag{29}$$

where

$$g(x,T)=\frac{165}{R(x,T)}e^{-Q_2/k_BT}+\frac{R(x,T)}{1+450x^2}e^{-Q_3/k_BT} \tag{30}$$

$$R(x,T)=\left(\sqrt{x^2+82e^{-\Delta H_{fO}/k_BT}}-x\right)^2 \tag{31}$$

This correlation is implemented in correlation Nr 33 of the etacrp.f95 routine for MOX fuel in the TRANSURANUS code.

3 Models for cladding properties

For what concerns the cladding modelling, dedicated models for the MYRRHA cladding steel (DIN 1.4970, of the 15-15Ti steels family and generally suitable for fast reactor pins) [68] have been implemented in TRANSURANUS v1m4j22 and used for MYRRHA simulations within the PATRICIA Project. These models concern the thermal and irradiation-induced creep, void swelling and time-to-rupture, applicable to ranges relevant for the current MYRRHA core design. They are recalled in what follows, while the detailed model derivation, assessment and application to MYRRHA irradiation scenarios are already published in [68, 69].

A novel correlation has been developed based on recent results of creep tests performed by the DeBeNe consortium on annealed and cold-worked 15-25% DIN 1.4970 [70], referring to the temperature range 600-750°C. In [70], a correlation tailored only on the non-aged specimen data was elaborated, exploiting an Arrhenius temperature dependence (i.e., exponential on the temperature). The original correlation herein proposed also features the Arrhenius functional form (like the standard TRANSURANUS model, by Többe [71]), but fitting the activation energy and other two model parameters on the whole DeBeNe dataset in order to consider both aged and non-aged specimens:

$$\dot{\varepsilon}_{\mathrm{th}} = \left(\sinh\left(0.0123\ \sigma_{\mathrm{eq}}\right)\right)^{2.332} \cdot \exp\left(-\frac{1.205 \cdot 10^5}{\mathrm{R} \cdot \mathrm{T}}\right) \tag{32}$$

where the equivalent thermal creep strain rate $\dot{\varepsilon}_{\mathrm{th}}$ is provided in h^{-1} and R is the gas constant (~ 8.314 J mol^{-1} K^{-1}). T (K) is the absolute temperature, σ_{eq} (MPa) the Von Mises equivalent stress.

Concerning the irradiation-induced creep strain rate, which dominates at the MYRRHA cladding working temperatures, few studies on DIN 1.4970 cladding steel can be found in the open literature. A data-driven approach has been pursued to derive a correlation based on the experimental data reported by Grossbeck et al. [72], for a cold-worked and aged DIN 1.4970 tested in the BR-2 reactor at 100 MPa. As suggested in [72], the irradiation creep strain rate data have been interpolated by means of a square root dependence on the neutron flux (best-fitting the considered associated data), while keeping the other dependences unchanged with respect to Többe's correlation (standard TRANSURANUS model) [71]:

$$\dot{\varepsilon}_{\mathrm{irr}} = 1.266 \cdot 10^{-15} \cdot \overline{\mathrm{E}} \cdot \sigma_{\mathrm{eq}} \cdot \sqrt{\phi} \tag{33}$$

where $\dot{\varepsilon}_{\mathrm{irr}}$ (h^{-1}) is the Von Mises equivalent irradiation creep strain rate, $\overline{\mathrm{E}}$ (MeV) is the mean neutron energy, ϕ (cm^{-2} s^{-1}) the neutron flux, σ_{eq} (MPa) is the Von Mises equivalent stress.

The state-of-the-art version of the TRANSURANUS code is equipped with a correlation for the time-to-rupture due to thermal creep accounting for the stress and temperature conditions existing in the cladding and based on the P parameter (a reformulation of the Larson-Miller parameter), considered suitable for 15-15Ti cladding steels [14, 73]. Significant thermal creep is not expected in the MYRRHA cladding under normal operating conditions (due to the low operative temperatures, 270°C - 450°C), but the incorporation in fuel performance codes of an advanced modelling is part of a wider development enabling the proper consideration of transient conditions. Available experimental data for annealed and cold-worked DIN 1.4970 [70, 74, 75] allowed the derivation of a novel and dedicated model. The Larson-Miller parameter (LMP, broadly used in literature [76, 77]) has been selected for the new approach, defined as:

$$\mathrm{LMP} = \mathrm{T} \cdot \left(C + \log_{10} \mathrm{t_R}\right) \tag{34}$$

where T (K) is the absolute temperature, t_R (h) is the time-to-rupture and *C* is a model parameter, equal to 17.6 for the MYRRHA cladding steel under consideration [70]. The two functional shapes suggested in [70] for two stress ranges (i.e., equivalent stress higher/lower than 1.7 MPa) have been adopted, while determining the correlation coefficients on the whole datasets from [70, 74, 75]. In addition, the two curves have been connected through a sigmoidal function ω, obtaining the LMP correlation as a function of the equivalent stress:

$$\omega = \frac{1}{2}\left[1 + \tanh\left(\frac{\sigma_{eq} - 52.47}{6.51}\right)\right] \tag{35}$$

$$\begin{aligned} \mathrm{LMP} = {} & [-6.41 \cdot 10^3 \cdot \log_{10}\sigma_{eq} + 3.22 \cdot 10^4] \cdot (1 - \omega(\sigma_{eq})) \\ & + \left[\left(\frac{2.64}{21.01} \cdot \left(\log_{10}\sigma_{eq} - 1.21\right) + 1\right) \cdot \right. \\ & \left. (22.01 - \exp\left(1.46 \cdot (\log_{10}\sigma_{eq} - 1.21)\right)) \cdot 10^3\right] \cdot \omega(\sigma_{eq}) \end{aligned} \tag{36}$$

where σ_{eq} (MPa) is the Von Mises equivalent stress.

For the void swelling of the cladding, specific models for DIN 1.4970, employed in the fuel performance code MACROS [78] and presented in Lemehov et al. [79], have been implemented in TRANSURANUS for the MYRRHA pin performance analysis:

$$\delta\left(\frac{\Delta V}{V}\right) = \dot{S}_0\left(\delta\Phi + \alpha \cdot \ln\left(\frac{1 + \exp\left(\frac{\Phi_0 - \Phi - \delta\Phi}{\alpha}\right)}{1 + \exp\left(\frac{\Phi_0 - \Phi}{\alpha}\right)}\right)\right) \tag{37}$$

where $\delta\left(\frac{\Delta V}{V}\right)$ (%) is the cladding swelling variation due to the fast (E > 0.1 MeV) neutron fluence increment $\delta\Phi$, starting from fluence Φ (both expressed in cm^{-2}). α is a constant equal to $1/(3 \cdot 10^{-23})$ cm^{-2}, while $\dot{S}_0$ ($\%/cm^{-2}$) and Φ_0 (cm^{-2}) are the swelling rate and the incubation fluence, respectively. $\dot{S}_0$ and Φ_0 (depending on the absolute temperature T (K)) are specifically modelled for two versions of the DIN1.4970: the “B” version which corresponds to a standard DIN1.4970, while the “L” version is swelling-strengthened, featured by a Si content up to 0.96% [79].

4 Models for coolant properties

Advanced models are also implemented in TRANSURANUS v1m4j22 and employed for the thermo-physical properties of the LBE coolant (e.g., thermal conductivity, specific heat, viscosity) of MYRRHA in PATRICIA. These models correspond to the recommendations provided by the latest NEA Handbook (2015 Edition) [80] and are recalled in Table 13.

The heat transfer coefficient between cladding and coolant is typically modelled in TRANSURANUS via the Ushakov correlation [81], of reference for lead / bismuth / lead-bismuth eutectic (LBE) coolants. Additional correlations suitable for LBE (i.e., those by Subbotin and Kazimi-Carelli, reviewed by [82] and recently by [83]) are now implemented in TRANSURANUS and available for e.g., sensitivity analyses (Table 14). Indeed, they prove to be more conservative compared to the Ushakov correlation, for example in the MYRRHA normal operation conditions targeted within the PATRICIA Project, since providing a lower Nusselt number (~ 20-25% lower) [83, 84].

Table 13: Correlations implemented in TRANSURANUS v1m4j22 for the thermo-physical properties of the LBE coolant [80] (T (K) = local temperature).

Property	Correlation	Range of applicability
Density (kg m^{-3})	$\rho = 11065 - 1.293 \cdot T$	[400, 1800] K
Thermal expansion (K^{-1})	$\alpha = 1/(8558 - T)$	[400, 1500] K
Specific heat (J kg^{-1} K^{-1})	$Cp = 164.8 + 3.94 \times 10^{-2} \cdot T + 1.25 \times 10^{-5} \cdot T^2 - 4.56 \times 10^{5} \cdot T^{-2}$	[400, 1100] K
Thermal conductivity (W m^{-1} K^{-1})	$k = 3.284 + 1.617 \times 10^{-2} \cdot T - 2.305 \times 10^{-6} \cdot T^2$	[400, 1200] K
Dynamic viscosity (Pa s)	$\mu = 4.94 \times 10^{-4} \cdot \exp(754.1/T)$	[400, 1300] K

Table 14: Selected literature correlations for the heat transfer to liquid metal coolants, applicable to fast reactor-type hexagonal lattice of fuel pins, implemented in TRANSURANUS v1m4j22 (Nu = Nusselt number, x = pitch-to-diameter ratio, Pe = Peclet number).

Correlation	Range of applicability	Fluid of applicability	Reference
$Nu = 7.55x - 20x^{-13} + 0.041x^{-2}Pe^{(0.56+0.19x)}$	$1 \leq Pe \leq 4000$ $1.3 \leq x \leq 2.0$	Pb, LBE	Ushakov et al. 1977 [81] Agosti et al. 2013 [85]
$Nu = 4.0 + 0.33x^{3.8}(Pe/100)^{0.86} + 0.16x^{5.0}$	$10 \leq Pe \leq 5000$ $1.1 \leq x \leq 1.4$	Na, Hg, Na-K	Kazimi and Carelli, 1976 [82]
$Nu = 0.58\left(2\sqrt{3}x^2/\pi - 1\right)^{0.55}Pe^{0.45}$	$80 \leq Pe \leq 4000$ $1.1 \leq x \leq 1.5$	LBE	Subbotin et al., 1965 [82]

5 Discussion

5.1 Melting (solidus) temperature modelling

The implementation of the material properties and correlations in the fuel performance codes based on information from WP4 and the open literature has also been the subject of some discussions during review meetings of the PATRICIA Project or organized separately by WP4 and WP5 (online). Some of the questions are still open and currently under investigation, as outlined below. The discussion provided in this section aims to provide an assessment of the state-of-the-art and achievements reported in this Deliverable and provides a basis for further developments.

The first question relates to the atomic-scale calculations contained in the PATRICIA Deliverable D4.3 [19, 49] and published by Labonne et al. [19] (shown as “our parametrization” in the figure below). The question relates to the evolution of the melting temperature evaluated at O/M = 2.00 that meets the experimental data by Epifano [24] and Latta and Fryxell [86] when applying a shift:

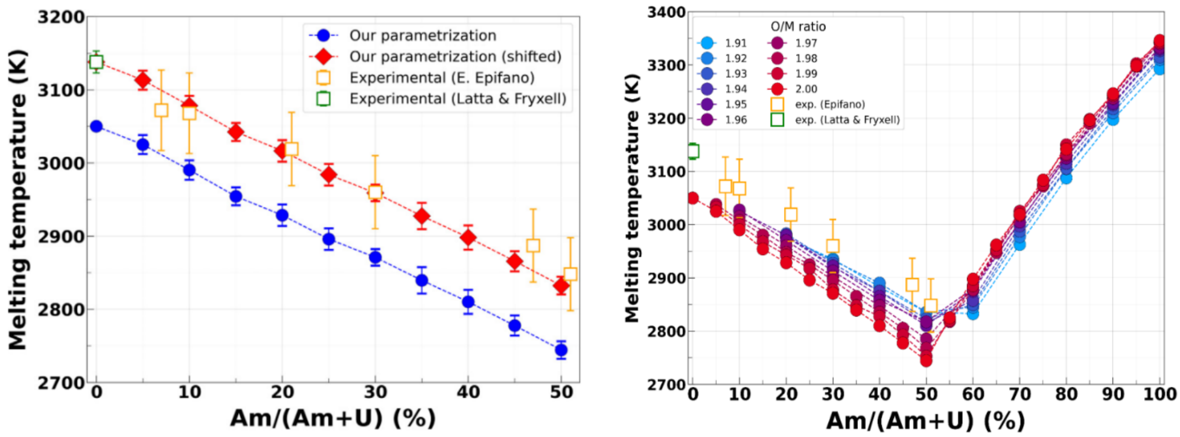

Figure 7: Behaviour of the melting (solidus) temperature of $(U,Am)O_2$ (left) and $(U,Am)O_{2-x}$ (right) as a function of the Am content, from atomic-scale calculations.

What could not be clarified is whether the curves reported in D4.3 for hypo-stoichiometric $(U,Am)O_{2-x}$ also require a shift. In principle a shift is also needed but needs to be clarified by means of additional atomic-scale calculations.

A second question is about the dependency of the melting (solidus) temperature as a function of the O/M ratio, raised when comparing the atomic scale calculations reported in D4.3 (Figure 8 - right) with the CAPLHAD data shared from WP4 to WP5 in June 2023 (Figure 8 - left). This revealed an opposite behaviour as a function of O/M for Am concentrations below 50%. Advanced CALPHAD approaches are currently leading to an increasing behaviour of the U-Am-O solidus temperature with decreasing O/M in the hypo-stoichiometry region, similarly to the U-Pu-O system according to the recent study by [18]. The U-Pu-O system behaviour is explained by the Pu stabilization effect in the hypo-stoichiometric mixed oxide due to the formation of oxygen vacancies and Pu^{3+} at high temperatures, leading to a minimum of the Gibbs energy curve. Additional investigations are showing the existence of a minimum in the Gibbs energy of U-Am-O with 20% Am, for O/M ~ 1.93, meaning that this composition is the most stable and that the curves of solidus/liquidus temperatures correspondingly show a maximum, potentially related to the formation of oxygen vacancies and Am^{3+} in $(U,Am)O_{2-x}$. Experimental measurements confirming these calculation results are needed. It must be recalled that the melting temperature of U-Am-O is currently experimentally unknown for O/M < 2 (hence CALPHAD models are empirically optimized in absence of data).

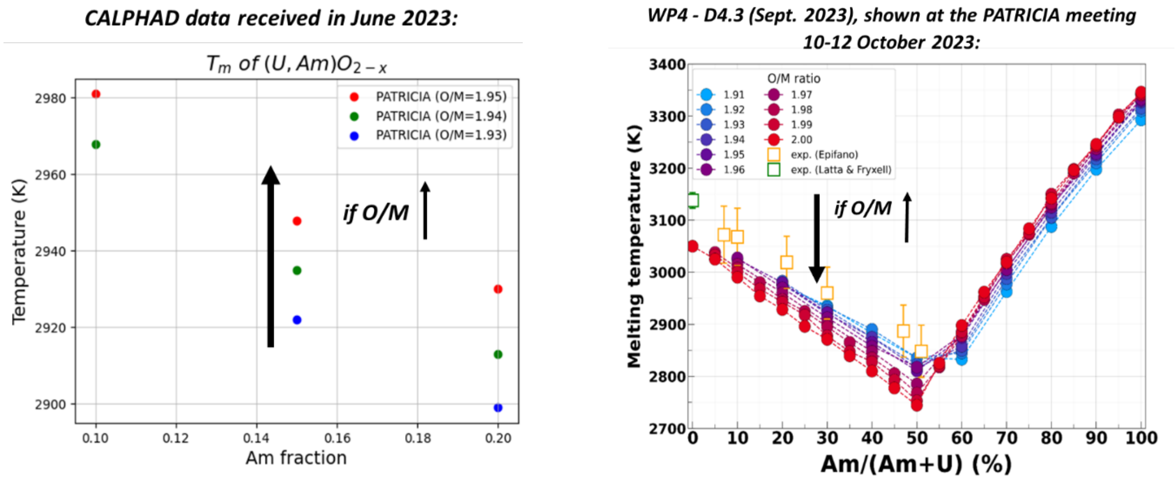

Figure 8: Behaviour of the melting temperature of $(U,Am)O_{2-x}$ as a function of the Am content, for different O/M values, as predicted by CALPHAD modelling (left) or atomic-scale calculations (right).

Additionally, it was indicated by B. Labonne (WP4) that further investigation of the atomic-scale results for Am contents > 50% is required to take into consideration a reduced value for the T_{melt} of AmO_2. This would also help to understand what might be the associated physical explanation, reflecting in e.g., a revised interatomic potential for Am to be employed in future calculations.

Further analysis of the former CALPHAD model results obtained in the frame of the former INSPYRE Project (Deliverable D1.4 "Advances on the margin to fuel melting behaviour of fast breeder MOX"[22]) for melting temperatures of $(U,Pu,Am)O_2$ compounds shows an underestimation of the solidus temperature when compared to measurements of melting temperatures of TRABANT and PHENIX fuels (shown in Figure 9 below). It was pointed out that, although difficulties in measurements of the solidus-liquidus points were reported, the values are still recommended as solidus values.

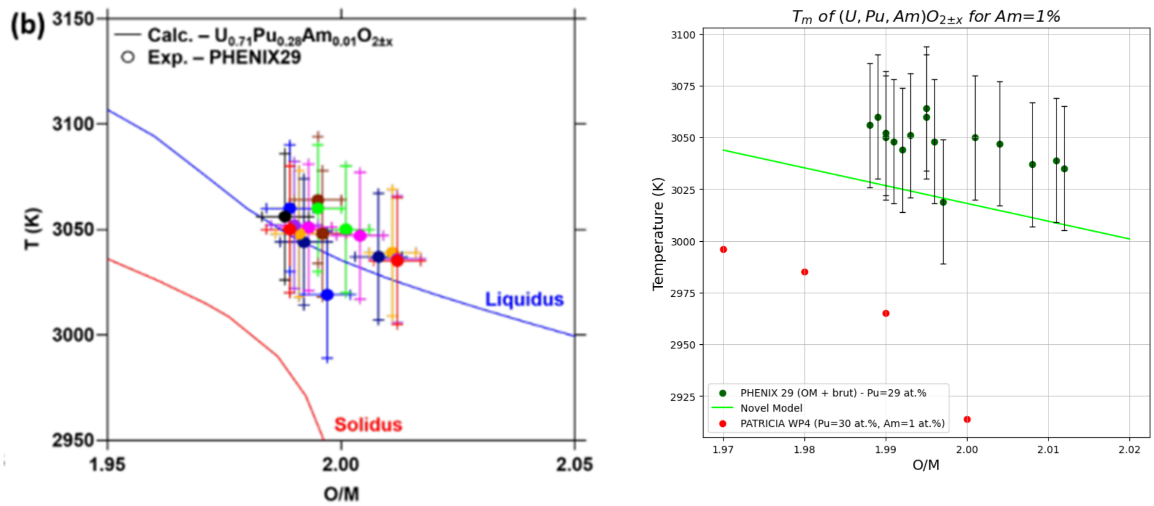

Figure 9: Experimental data on the melting temperature (solidus / liquidus) of Phénix U-Pu-Am-O fuel, compared to part of the phase diagram from CALPHAD obtained during the former INSPYRE Project (left), while to the novel model proposed (Section 2.2) and to novel CALPHAD data from PATRICIA WP4 for similar fuel composition (right).

It remains to be clarified whether one should consider the experimental results (together with data from WP4) in light of the questionable reliability of these solidus temperature points. It is still not well established whether the single temperature of thermal arrest (instead of a double temperature arrest during heat-up and subsequent cooling) detected during the laser heating tests represents the solidus or liquidus temperature. Consequently, large uncertainties are still associated to the solidus/liquidus temperatures of Am-containing MOX.

5.2 Specific heat modelling

Another topic subject to discussion is about the specific heat capacity of $(U,Am)O_2$ fuel. The values provided by WP4 increase slightly when moving from the hypo-stoichiometry region towards O/M = 2.00, as shown in Figure 10.

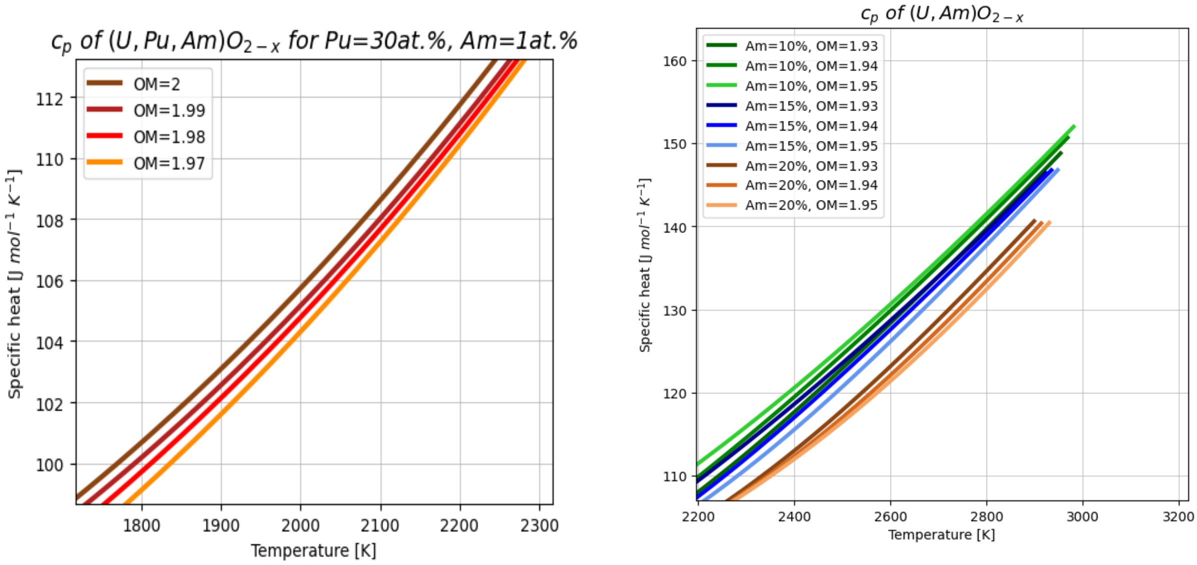

Figure 10: Behaviour of the specific heat capacity of U-Pu-Am-O fuels (left) and U-Am-O fuels (right), as a function of the temperature, as provided by PATRICIA WP4.

It is unclear whether this slight trend is confirmed for both U-Am-O and U-Pu-Am-O, as well as for $(U,Am)O_2$ at different Am contents, especially at higher temperatures. Nevertheless, there is no clear experimental result available showing the trend of the specific heat capacity of these systems as a function of the O/M ratio. A very small effect is indicated by the only experimental data available on $(U,Pu)O_{2-x}$ (recalled in Table 9), hence the same is currently considered for Am-bearing oxides.

Atomic-scale calculations of specific heat capacity were also compared to the available experimental data on $(U,Am)O_2$, such as those from Epifano et al. [56], Pavlov et al. [42], or Valu et al. [51], at O/M = 2.00 or slight hypo-stoichiometry. The comparison indicates a small effect of O/M on the specific heat capacity also in the lower temperature range, confirmed by both measurements and calculations. Furthermore, atomic-scale calculations at low temperatures currently show a systematic underestimation of the experimental specific heat capacity (Figure 11 – left), not just for Am-bearing oxides but also for U-Pu-O compositions. This is confirmed by the enthalpy increment data, whose slope is significantly lower from atomic-scale calculations compared to measurements by means of calorimetry techniques. A correction of the atomic-scale data is hence suggested to match the experimental data, corresponding to a shift to higher specific heat values (linked to a modification of the interatomic potential chosen for the simulations [87]).

Model developments in Task 5.1 of the PATRICIA Project (Section 2.3) also reveal a peculiar behaviour of the specific heat capacity of $(U,Am)O_2$ at 50% Am, especially at high temperature where the so-called Bredig transition is still predicted by the atomic-scale simulations (Figure 11), but it is flattened compared to lower Am compositions [87]. This is in principle of interest for the safety analysis by means of fuel performance codes, although the focus remains for the moment on values of Am content between 10 and 20% in the U-Am-O fuel system.

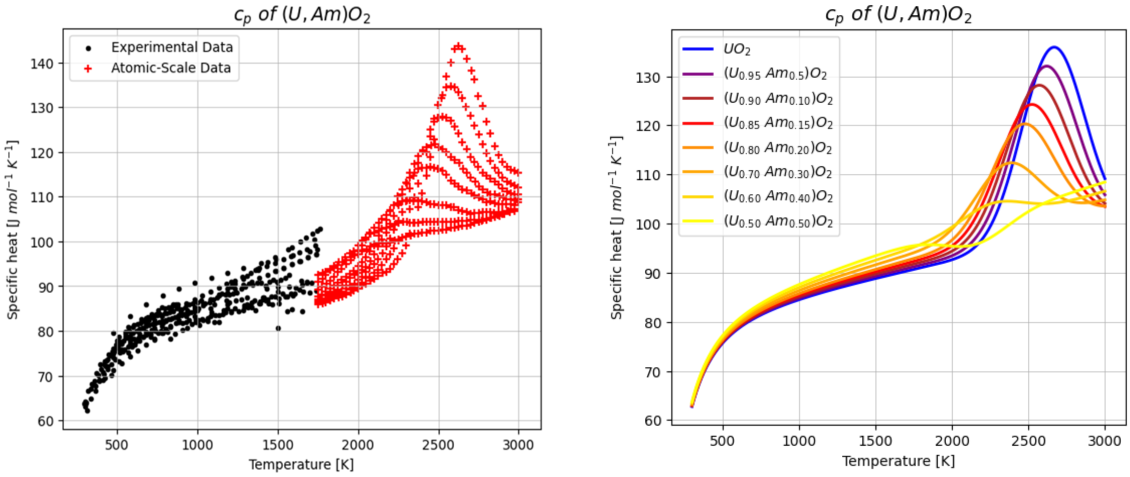

Figure 11: Experimental and atomic-scale data for $(U,Am)O_2$ over the entire temperature range up to fuel melting (left), and behaviour of the resulting model up to 50 at.% Am.

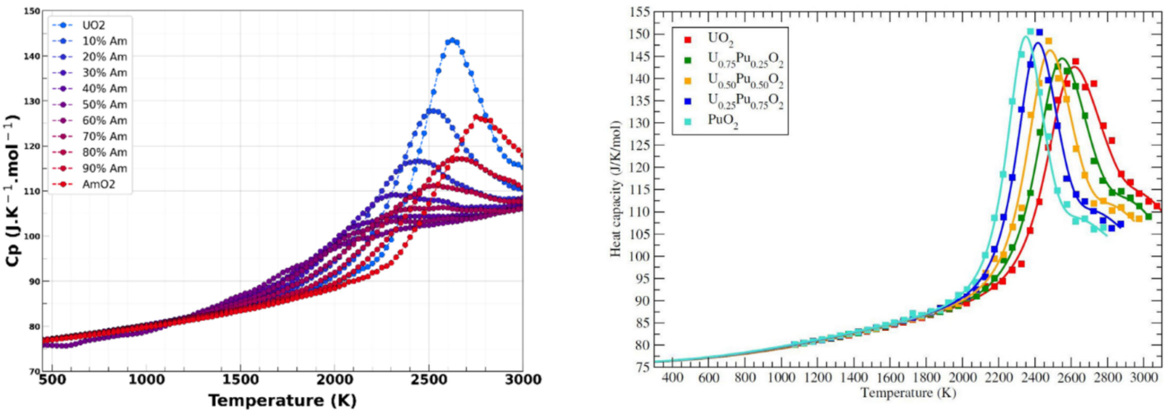

Figure 12: Atomic-scale data for the specific heat capacity over the entire temperature range up to fuel melting, as calculated during the INSPYRE Project (left) and during the PATRICIA Project (right).

Further differences were observed when comparing results from the PATRICIA Project (Deliverable 4.3) with some obtained in the frame of the former INSPYRE Project [48], when the Pu and Am concentrations increase (Figure 12). It is unclear for the moment what the reason is for these differences, although it should be underlined that their impact in the simulations considered in WP5 (past irradiation experiments of Am-bearing fuels) and WP6 (irradiation of Am-bearing fuels in MYRRHA) is negligible.

6 Conclusions and recommendations

In the frame of Task 5.1 the PATRICIA Project, specific modelling advancements concerning fuel thermo-physical properties and behaviour (creep) were carried out. They are recommended for further use and therefore implemented in the fuel performance codes TRANSURANUS and GERMINAL to extend their applicability and assessment to a broader set of fuel materials and fast reactor irradiation conditions.

The safety-relevant oxide fuel properties modelled and implemented include: (i) melting (solidus) temperature correlations for minor actinide (Am, Np)-bearing fuels implemented in TRANSURANUS; (ii) thermal conductivity correlations for minor actinide (Am, Np)-bearing fuels implemented in both TRANSURANUS and GERMINAL, and additionally advanced models for U-Pu-Am-O and U-Am-O fuels in TRANSURANUS; (iii) a heat capacity model for U-Pu MOX fuels extended to account for the fuel Am content, implemented in TRANSURANUS; and (iv) a more mechanistic model for oxide fuel creep in TRANSURANUS. The first two properties benefited from the developments in WP4 based on molecular dynamics and CALPHAD simulations. Some remaining questions and open points concerning the properties discussed in this report will be taken into consideration in future follow-up works and uncertainty analyses via code simulations.

It should be pointed out that the modelling improvements of the SCIANTIX module, for the more detailed and mechanistic description of inert gas behaviour and fuel microstructure evolution, have been coupled with the TRANSURANUS and GERMINAL codes. This is out of the scope of this Deliverable, but it is reported separately in Deliverable 5.2.

As far as the cladding properties are concerned, dedicated correlations for the MYRRHA cladding steel (DIN 1.4970, of the 15-15Ti steels family) were implemented in TRANSURANUS and used for MYRRHA simulations. More precisely, the laws considered are the thermal and irradiation-induced creep, void swelling and time-to-rupture, applicable to ranges relevant for the current MYRRHA core design.

Finally, advanced correlations for thermo-physical properties of the LBE coolant were also implemented in TRANSURANUS. On the one hand, the thermal conductivity, specific heat, and viscosity were derived on the basis of the recommendations provided by the latest NEA Handbook. On the other hand, the heat transfer coefficient between cladding and coolant is modelled in TRANSURANUS via the Ushakov correlation. Other correlations suitable for LBE, from Subbotin and Kazimi-Carelli, have also been implemented in the TRANSURANUS code for a sensitivity analysis.

The model improvements outlined above enable a reliable application of the fuel performance codes to the advanced fuel concepts for fast reactor, e.g., for the preliminary design and assessment of the overall pin performance both during normal operation and transient / accidental conditions . This will be verified in the comparison with experimental data in Task 5.3 and further demonstrated on the MYRRHA scenarios considered in WP6.

7 References

1. *Lassmann, K., TRANSURANUS: a fuel rod analysis code ready for use. 1992.* ***188****: p. 295-302.*
2. *Magni, A., et al., Chapter 8 - The TRANSURANUS fuel performance code, in Nuclear Power Plant Design and Analysis Codes, J. Wang, et al., Editors. 2021, Woodhead Publishing. p. 161-205.*
3. *Lainet, M., et al., GERMINAL, a fuel performance code of the PLEIADES platform to simulate the in-pile behaviour of mixed oxide fuel pins for sodium-cooled fast reactors. Journal of Nuclear Materials, 2019.* ***516****: p. 30-53.*
4. *Michel, B., et al., Chapter 9 - Two fuel performance codes of the PLEIADES platform: ALCYONE and GERMINAL, in Nuclear Power Plant Design and Analysis Codes, J. Wang, et al., Editors. 2021, Woodhead Publishing. p. 207-233.*
5. *PATRICIA - Partitioning And Transmuter Research Initiative in a Collaborative Innovation Action. European Union's Horizon 2020 Research and Innovation programme 2020; Available from: https://patricia-h2020.eu/.*
6. *D'Agata, E., et al., SPHERE: Irradiation of sphere-pac fuel of UPuO$_{2-x}$ containing 3% Americium. Nuclear Enegineering and Design, 2014.* ***275****: p. 300-311.*
7. *D'Agata, E., et al., The MARINE experiment: Irradiation of sphere-pac fuel and pellets of UO2−x for americium breading blanket concept. Nuclear Engineering and Design, 2017.* ***311****: p. 131-141.*
8. *Magni, A., et al., Modelling and assessment of thermal conductivity and melting behaviour of MOX fuel for fast reactor applications. Journal of Nuclear Materials, 2020.* ***541****: p. 152410.*
9. *Philipponneau, Y., Thermal conductivity of (U,Pu)O$_{2-x}$ mixed oxide fuel. Journal of Nuclear Materials, 1992.* ***188****: p. 194-197.*
10. *Carbajo, J.J., et al., A Review of the Thermophysical Properties of MOX and UO$_2$ Fuels. Journal of Nuclear Materials, 2001.* ***299****: p. 181-198.*
11. *Sobolev, V., et al., Modelling the behaviour of oxide fuels containing minor actinides with urania, thoria and zirconia matrices in an accelerator-driven system. Journal of Nuclear Materials, 2003.* ***319****: p. 131-141.*
12. *Kato, M., et al., Physical properties and irradiation behavior analysis of Np- and Am-Bearing MOX Fuels. J. Nucl. Sci.Technol., 2011.* ***48****: p. 646-653.*
13. *Prieur, D., et al., Linear thermal expansion, thermal diffusivity and melting temperature of Am-MOX and Np-MOX. Journal of Alloys and Compounds, 2015.* ***637****: p. 326-331.*
14. *Lassmann, K., et al., TRANSURANUS Handbook, Copyright ⓒ 1975--2022. 2022: European Commission, Joint Research Centre, Karlsruhe.*
15. *Magni, A., et al., Modelling of thermal conductivity and melting behaviour of minor actinide-MOX fuels and assessment against experimental and molecular dynamics data. Journal of Nuclear Materials, 2021.* ***557****: p. 153312.*
16. *Manara, D., et al., Melting of stoichiometric and hyperstoichiometric uranium dioxide. Journal of Nuclear Materials, 2005.* ***342****: p. 148-163.*
17. *Martin, P., et al., Preparing ESNII for HORIZON 2020 - Deliverable D7.5.1 - Catalog on MOX properties for fast reactors. 2017. p. 1-174.*
18. *Fouquet-Métivier, P., et al., Investigation of the solid/liquid phase transitions in the U–Pu–O system. Calphad, 2023.* ***80****: p. 102523.*
19. *Labonne, B., S. Orlat, and M. Bertolus, Development of an interatomic potential for mixed uranium-americium oxides and application to the determination of the structural and thermodynamic properties of (U,Am)O$_2$ with americium contents below 50%. Journal of Nuclear Materials, 2023.* ***579****: p. 154390.*
20. *Kato, M., Melting temperatures of oxide fuel for fast reactors, in ICAPP '09. 2009: Tokyo, Japan. p. paper 9451.*
21. *De Bruycker, F., et al., On the melting behaviour of uranium/plutonium mixed dioxides with high-Pu content: A laser heating study. Journal of Nuclear Materials, 2011.* ***419****(1): p. 186-193.*
22. *Gueneau, C., et al., Advances on the margin to fuel melting behivour of fast breeder MOX, in INSPYRE project deliverables, M. Bertolus, Editor. 2023: Brussels, Belgium.*

23. *Prieur, D., et al., Melting behaviour of americium-doped uranium dioxide. The Journal of Chemical Thermodynamics, 2016. **97**: p. 244-252.*
24. *Epifano, E., et al., Melting behaviour of uranium-americium mixed oxides under different atmospheres. The Journal of Chemical Thermodynamics, 2020. **140**: p. 105896.*
25. *Morimoto, K., et al., Thermal conductivity of (U,Pu,Np)O2 solid solutions. Journal of Nuclear Materials, 2009. **389**(1): p. 179-185.*
26. *Morimoto, K., et al., Thermal conductivities of (U, Pu, Am)O_2 solid solutions. Journal of Alloys and Compounds, 2008. **452**(1): p. 54-60.*
27. *Morimoto, K., et al., Thermal conductivities of hypostoichiometric (U, Pu, Am)O2-x oxide. journal of Nuclear Materials, 2008. **374**(3): p. 378-385.*
28. *Yokoyama, K., et al., Measurements of thermal conductivity for near stoichiometric (U0.7-zPu0.3Amz)O2 (z = 0.05, 0.10, and 0.15). Nuclear Materials and Energy, 2022. **31**: p. 101156.*
29. *McKinney, C., et al., Three-dimensional microstructural characterization of FBR MOX fuel and the contribution of microstructural features to the thermal conductivity of the fuel. Journal of Nuclear Materials, 2022. **572**: p. 154073.*
30. *Bonev, P., et al., New recommendation for the thermal conductivity of irradiated (U, Pu)O_2 fuels under fast reactor conditions. Comparison with recent experimental data. Journal of Nuclear Materials, 2023. **577**: p. 154326.*
31. *Colle, J.-Y., et al., Comparative study of fission product release of homogeneous and heterogeneous high-burn up MOX fuel by Knudsen Effusion Mass Spectrometry supported by EPMA, SEM/TEM and thermal diffusivity investigations. Journal of Nuclear Materials, 2023. **578**: p. 154340.*
32. *Kitano, K. and H. Akiyama, Research on the properties of high-burnup and high plutonium content mixed-oxide fuels. Journal of Nuclear Materials, 2022. **572**: p. 154075.*
33. *Horii, Y., et al., Thermal conductivity measurement of uranium–plutonium mixed oxide doped with Nd/Sm as simulated fission products. Journal of Nuclear Materials, 2024. **588**: p. 154799.*
34. *Vigier, J.-F., et al., Synthesis and characterization of homogeneous (U,Am)O2 and (U,Pu,Am)O2 nanopowders. CrystEngComm, 2022. **24**(36): p. 6338-6348.*
35. *Fukushima, S., et al., Thermal conductivity of near-stoichiometric (U, Nd)O2, (U, Sm)O2 and (U, Eu)O2 solid solutions. Journal of Nuclear Materials, 1983. **114**(2): p. 312-325.*
36. *Ronchi, C., et al., Thermal Conductivity of Uranium Dioxide up to 2900 K from Simultaneous Measurement of the Heat Capacity and Thermal Diffusivity. Journal of Applied Physics, 1999. **85**: p. 776-789.*
37. *Ronchi, C., et al., Effect of Burn-up on the Thermal Conductivity of Uranium Dioxide up to 100 000 $MWdt^{-1}$. Journal of Nuclear Materials, 2004. **327**(1): p. 58-76.*
38. *Vălu, O.S., et al., Heat capacity, thermal conductivity and thermal diffusivity of uranium–americium mixed oxides. Journal of Alloys and Compounds, 2014. **614**: p. 144-150.*
39. *Lucuta, P.G., Hj. Matzke, and I.J. Hastings, A pragmatic approach to modelling thermal conductivity of irradiated UO_2 fuel: Review and recommendations. Journal of Nuclear Materials, 1996. **232**: p. 166-180.*
40. *Jossou, E., et al., Thermophysical properties of (U_xAm_{1-x})O_2 MOX fuel. Computational Materials Science, 2020. **172**: p. 109324.*
41. *Prieur, D., et al., Local Structure and Charge Distribution in Mixed Uranium–Americium Oxides: Effects of Oxygen Potential and Am Content. Inorganic Chemistry, 2011. **50**(24): p. 12437-12445.*
42. *Pavlov, T.R., et al., Measurement and interpretation of the thermo-physical properties of UO_2 at high temperatures: The viral effect of oxygen defects. Acta Materialia, 2017. **139**: p. 138-154.*
43. *Middleburgh, S.C., et al., Swelling due to fission products and additives dissolved within the uranium dioxide lattice. Journal of Nuclear Materials, 2012. **427**: p. 359-363.*
44. *Nishi, T., et al., Heat capacities and thermal conductivities of AmO_2 and $AmO_{1.5}$. Journal of Nuclear Materials, 2011. **414**(2): p. 109-113.*

45. Lebreton, F., et al., *Peculiar Behavior of $(U,Am)O_{2-\delta}$ Compounds for High Americium Contents Evidenced by XRD, XAS, and Raman Spectroscopy. Inorganic Chemistry, 2015.* ***54****(20): p. 9749-9760.*
46. Vauchy, R., et al., *Lattice parameters of fluorite-structured uranium–americium mixed oxides. Journal of Nuclear Materials, 2023.* ***584****: p. 154576.*
47. Longoni, L., *Analysis of an Am-bearing experimental fuel pin in a MYRRHA transient scenario, in Nuclear Engineering. 2022, Politecnico di Milano: Milan, Italy. p. 108.*
48. Bathellier, D., et al., *A new heat capacity law for UO_2, PuO_2 and $(U,Pu)O_2$ derived from molecular dynamics simulations and useable in fuel performance codes. Journal of Nuclear Materials, 2021.* ***549****: p. 152877.*
49. Rochedy, M., et al., *Measurements and atomic scale calculations in U-Pu-Am-Np-O systems. 2023.*
50. Fink, J.K., *Thermophysical properties of uranium dioxide. Journal of Nuclear Materials, 2000.* ***279****(1): p. 1 - 18.*
51. Valu, O.S., et al., *The high temperature heat capacity of the $(Th,Pu)O_2$ system. J. Chem. Thermodynamics, 2014.* ***68****: p. 122-127.*
52. Oetting, F.L., *The chemical thermodynamics of nuclear materials. VII. the high-temperature enthalpy of plutonium dioxide. Journal of Nuclear Materials, 1982.* ***105****(2): p. 257-261.*
53. Kandan, R., et al., *Calorimetric measurements on uranium–plutonium mixed oxides. Journal of Nuclear Materials, 2004.* ***324****(2): p. 215-219.*
54. Kandan, R., et al., *Calorimetric measurements on plutonium rich (U,Pu)O2 solid solutions. Thermochimica Acta, 2008.* ***472****(1): p. 46-49.*
55. *Thermo-Physical Materials Properties Database of LWRs and HWRs, IAEA, Editor. 2023, IAEA.*
56. Epifano, E., et al., *High temperature heat capacity of (U, Am)O2±x. Journal of Nuclear Materials, 2017.* ***494****: p. 95-102.*
57. Solomon, A.A., J.L. Routbort, and J.C. Voglewede, *Fission-induced creep of UO_2 and its significance to fuel-element performance. 1971, Argonne National Laboratory.*
58. Többe, H. *1975. p. 102.*
59. Matthews, J.R. and M.W. Finnis, *Irradiation creep models — an overview. Journal of Nuclear Materials, 1988.* ***159****: p. 257-285.*
60. Bernard, A., et al., *Safety Requirements For Pellet-Clad Interaction In France – New Approach Developed By EDF, in Techn. Meeting on Experimentation, Modelling and Methodologies Applied to Support the Flexible Operation of Nuclear Power Plants. Progress on Pellet-Caldding Interaction and Stress Corrosion Cracking. 2019, IAEA: Aix-en-Provence, France. p. 103-113.*
61. Portelette, L., et al., *Viscoplastic behavior of a porous polycrystal with similar pore and grain sizes: Application to nuclear MOX fuel materials. International Journal of Solids and Structures, 2022.* ***236-237****: p. 111316.*
62. Caillot, L., C. Nonon, and V. Basini. *Out-of-pile and In-pile Viscoplastic Behaviour of Mixed-oxide Fuels. in Pellet-clad Interactions in Water Reactor Fuels. 2004. Aix-en Provence, France.*
63. Malygin, V.B., et al., *Recommendations for calculating the characteristics of thermal creep of mixed uranium–plutonium oxide fuel when analyzing fuel-element serviceability. Atomic Energy, 2010.* ***108****(1): p. 15-20.*
64. Malygin, V.B., et al., *Recommendations for calculating the thermal creep properties of uranium dioxide when analyzing fuel-element serviceability. Atomic Energy, 2009.* ***107****(6): p. 381-386.*
65. Malygin, V.B., et al., *Recommendations for calculating the rate of irradiation-induced creep of oxide fuel when analyzing fuel-element serviceability. Atomic Energy, 2010.* ***108****(2): p. 121-126.*
66. Terrani, K.A., et al., *Uniform corrosion of FeCrAl alloys in LWR coolant environments. Journal of Nuclear Materials, 2016.* ***479****: p. 36-47.*
67. Klouzal, J. and V. Matocha, *Validation and application of TRANSURANUS for the CEZ NPPs, in Towards nuclear fuel modelling in the various reactor types across Europe, P. Van Uffelen, A. Schubert , and J. van de Laar, Editors. 2015, European Commission: Karlsruhe, Germany.*
68. Magni, A., et al., *Extension and application of the TRANSURANUS code to the normal operating conditions of the MYRRHA reactor. Nuclear Engineering and Design, 2022.* ***386****: p. 111581.*

69. *Magni, A., et al., Analysis of the performance of driver MOX fuel in the MYRRHA reactor under Beam Power Jump transient irradiation conditions. 2023.* ***414****: p. 112589.*
70. *Cautaerts, N., et al., Thermal creep properties of Ti-stabilized DIN 1.4970 (15-15Ti) austenitic stainless steel pressurized cladding tubes. Journal of Nuclear Materials, 2017.* ***493****: p. 154-167.*
71. *Többe, H., Das Brennstabrechenprogramm IAMBUS zur Auslegung von Schellbrüter Brennstäben, Interatom, Editor. 1975. p. 102.*
72. *Grossbeck, M.L., K. Ehrlich, and C. Wassilew, An assessment of tensile, irradiation creep, creep rupture, and fatigue behavior in austenitic stainless steels with emphasis on spectral effects. Journal of Nuclear Materials, 1990.* ***174****(2): p. 264-281.*
73. *Luzzi, L., et al., Modeling and Analysis of Nuclear Fuel Pin Behavior for Innovative Lead Cooled FBR, . 2014.*
74. *Schroeder, H., In-beam creep rupture properties of DIN 1.4970 austenitic stainless steel at 873 K. Journal of Nuclear Materials, 1986.* ***141-143****: p. 476-481.*
75. *Yamamoto, N. and H. Schroeder, In-beam creep rupture properties of cold-worked DIN 1.4970 and AISI 316 L at 873 K. Journal of Nuclear Materials, 1988.* ***155-157****: p. 1043-1048.*
76. *Larson, F.R. and J. Miller, Time-Temperature Relationship for Rupture and Creep Stresses, in ASME. 1952. p. 765-771.*
77. *Luzzi, L., et al., Application of the TRANSURANUS code for the fuel pin design process of the ALFRED reactor. Nuclear Engineering and Design, 2014.* ***277****: p. 173-187.*
78. *Lemehov, S.E., et al., MACROS benchmark calculations and analysis of fission gas release in MOX with high content of plutonium. Progress in Nuclear Energy, 2012.* ***57****: p. 117-124.*
79. *Lemehov, S.E., V.P. Sobolev, and M. Verwerft, Predicting thermo-mechanical behaviour of high minor actinide content composite oxide fuel in a dedicated transmutation facility. Journal of Nuclear Materials, 2011.* ***416****(1): p. 179-191.*
80. *OECD/NEA, Handbook on Lead-Bismuth Eutectic Alloy and Lead Properties, Materials Compatibility, Thermal-Hydraulics and Technologies. 2015.*
81. *Ushakov, P.A., A.V. Zhukov, and M.M. Matyukhin, Heat transfer to liquid metals in regular arrays of fuel elements High Temperatures - High Pressures, 1977 ; translated from Teplofizika Vysokikh Temperatur 15 (5), 1027-1033.* ***15****: p. 868-873.*
82. *Mikityuk, K., Heat Transfer to Liquid Metal: Review of Data and Correlations for Tube Bundles. Nuclear Engineering and Design, 2009.* ***239****: p. 680-687.*
83. *Di Gennaro, M., et al., OpenFOAM-informed TRANSURANUS simulation of the fuel pin behaviour in the MYRRHA reactor during BPJ transient scenario, in 16th Information Exchange Meeting on Actinide and Fission Product Partitioning and Transmutation (16IEMPT). 2023, OECD Nuclear Energy Agency: Boulogne-Billancourt, France. p. Paper S05.06.*
84. *Luzzi, L., et al., Performance analysis and helium behaviour of Am-bearing fuel pins for irradiation in the MYRRHA reactor. Nuclear Engineering and Design, 2023: p. submitted.*
85. *Agosti, F., et al., Heat transfer correlations for liquid metal cooled fast reactors. 2013, Politecnico di Milano: Milan, Italy.*
86. *Latta, R.E. and R.E. Fryxell, Determination of solidus-liquidus temperatures in the* uo_{2+x} *system (−0.50<x<0.20). Journal of Nuclear Materials, 1970.* ***35****(2): p. 195-210.*
87. *Labonne, B., S. Orlat, and M. Bertolus, Development of an interatomic potential for mixed uranium-americium oxides and application to the determination of the structural and thermodynamic properties of (U,Am)*O_2 *with americium contents below 50%. Journal of Nuclear Materials, 2024.* ***in preparation****.*